PROCEEDINGS A

royalsocietypublishing.org/journal/rspa

Research

Cite this article: Brini F, Seccia L. 2022 Acceleration waves and oscillating gas bubbles modelled by rational extended thermodynamics. *Proc. R. Soc. A* **478**: 20220246.
https://doi.org/10.1098/rspa.2022.0246

Received: 13 April 2022
Accepted: 3 October 2022

Subject Areas:
fluid mechanics, wave motion, thermodynamics

Keywords:
acceleration waves, rational extended thermodynamics, oscillating gas bubbles, dynamic pressure, polyatomic gas

Author for correspondence:
F. Brini
e-mail: francesca.brini@unibo.it

Acceleration waves and oscillating gas bubbles modelled by rational extended thermodynamics

F. Brini[1] and L. Seccia[2]

[1]University of Bologna, Department of Mathematics and AM, via Saragozza, 8, Bologna, Italy
[2]University of Bologna, Department of Mathematics and AM, via Fontanelle, 40, Forlì, Italy

FB, 0000-0002-0131-0727

The study of acceleration waves for a rarefied polyatomic gas is carried out in planar, cylindrical and spherical geometry referring to the rational extended thermodynamics theory with 14 moments. The case of a rarefied monatomic gas is determined as a limit case, and the role of geometry and molecular degrees of freedom is investigated. In addition, the behaviour of an acceleration wave travelling inside an oscillating gas bubble is modelled by the 14-moment PDE system under adiabatic condition. We show that dissipation combined with hyperbolicity tends to inhibit shock formation, and that the dynamic pressure cannot be zero inside the oscillating bubble. This fact can produce observable effects even in the Navier–Stokes approximation, if the gas exhibits high bulk viscosity.

1. Introduction

The term acceleration wave (from now on AW) indicates a propagating surface across which all the field variables are continuous, while the first derivatives of at least one field variable exhibit a jump [1–3]. Due to this property, such waves are also called weak discontinuities. AWs can be generated in different materials and a large literature is devoted to this topic and to its application. For the sake of brevity, we quote here only some works related to gases [4–11] (and the references therein). In gases, AWs are produced by a perturbation, which could be caused for instance by a piston during its accelerated motion.

THE ROYAL SOCIETY PUBLISHING

In recent decades, the modelling of gas phenomena through hyperbolic PDE systems that predict the presence of finite propagation velocities (unlike parabolic differential systems) is increasingly frequent.

The analysis of the phenomena related to the acceleration waves reveals that together with hyperbolicity, the presence of dissipative terms is also mandatory. In fact, it has been shown that conservation laws provide for the transformation of an AW into a shock wave for any value of the initial amplitude [3,7,12], in contrast to the experimental evidence [13]. In a better model of balance laws, on the contrary, it is usually possible to identify a critical value of the initial amplitude below which the acceleration wave does not turn into a shock [2–4,7–9]. This modelling is consistent with experimental evidence if the threshold values for jump formation are sufficiently high. In this respect, the AWs represent an important test bed for a gas theory.

Rational extended thermodynamics (RET) is a recent but now well-consolidated theory that has already shown the ability to predict far-from-equilibrium phenomena and rapid changes in gases. The theory was first introduced for monatomic gases with the pioneering works by Müller, Ruggeri and other researchers [14] and then, more recently, it was extended to polyatomic gases by Ruggeri *et al.* [15,16]. In all cases, this kind of model is based on the idea that the independent field variables are both the usual equilibrium variables (mass density, momentum and energy) and non-equilibrium quantities, such as stress tensor, dynamic pressure and heat flux. The corresponding field equations turn out to be hyperbolic balance laws, compatible with universal physical principles like entropy and relativity principles. Grad 13-moment theory can be seen as a particular case of RET theories for monatomic gases. A good experimental agreement has been obtained for several gas phenomena through RET models [14–16] and for this reason, it is natural to think of applying it also to complex phenomena such as those we will face in the second part of this paper.

The behaviour of planar AWs in monatomic rarefied gases described by RET was already studied in many cases [8–11] and there is also a preliminary analysis for a polytropic gas described by a RET system with only six fields [15]. All the results confirm that shock formation is physically unlikely. The first aim of the present paper is to test the polyatomic RET theory with 14 moments and study the evolution of AWs in different geometries and for different molecular degrees of freedom.

Spherical AWs, travelling towards the centre, represent a special issue, as was already observed by Lindsay & Straughan [5] and Greenspan & Nadim [17] for different sets of equations. In particular, [17] is developed within the field of the oscillating gas bubbles and has inspired the studies presented here. We realized that RET have never been tested in the complex framework of the oscillating gas bubbles and the mixture of hyperbolicity and dissipation of such a theory could make the difference. The aim of this paper is not to solve the well-known open questions related to bubbles phenomena, but rather to approach this special world with RET in a preliminary, elementary and simplified way.

A gas bubble within a liquid can be generated by mechanical, acoustic or optical devices. In many cases, bubbles are not present as a single isolated object, but they appear in large numbers, as for bubbles produced by ship propellers and studied by Lord Rayleigh, who investigated their cavitation effect for the first time in 1917 [18]. Over the years, the behaviour of multi-bubble structure driven by an acoustical field was the topic of several studies, due to the surprising effects observed experimentally. As a matter of fact, bubbles react to a periodical acoustic signal with nonlinear oscillations that can give rise to deterministic chaos and, under very specific conditions, to light emission, the so called sonoluminescence (SL) effect. The description of bubble dynamics involves different research fields, such as hydrodynamics, acoustics, heat and mass transfer, chemistry and sonochemistry, dynamical systems and quantum physics. More recently, different methods have been developed for generating a single bubble in a liquid, among which we mention a focused laser radiation pulse and the irradiation with a standing acoustic wave (acoustic trap, the very popular technique ensuring bubble stability). This fact has increased the literature about bubble dynamics, cavitation and SL, and we are not able here to quote even a fraction of all the books and papers published in the last 50 years on this topic, which turned

out to be several thousands. We recall among others the review papers [19–28] and the references therein, stressing the relevant application results, for example those related to sonochemistry [25] and medicine [29].

The paper is organized as follows. In §2, we will introduce the main ideas of RET, while the AW theory is presented in §3 and applied to RET theory with 14 moments in §4. In §5, we summarize some results about oscillating gas bubbles and have a first look at the topic through RET. Sections 6 and 7 focus on AW travelling in oscillating bubbles filled with monatomic and polyatomic gases. The results are analysed in §8 and some conclusions are presented in §9.

2. The balance laws of rational extended thermodynamics

RET theories for rarefied polyatomic gases were recently introduced following two different approaches [15]. On the one hand, it is possible to construct a phenomenological model, as first done by Arima *et al.* in [16] requiring the validity of universal physical principles, such as the Galilean invariance and the entropy principle. On the other hand, the hyperbolic equations can be derived referring to the kinetic theory [30] and imposing that the distribution function associated with a polyatomic gas depends not only on time (t), space ($\mathbf{z}=(z_1,z_2,z_3)$) and microscopic velocity ($\mathbf{c}=(c_1,c_2,c_3)$), but also on a continuous variable I ($I\in[0,\infty)$) that represents the internal modes of the molecules. Such a function ($f=f(t,\mathbf{z},\mathbf{c},I)$) satisfies a generalized Boltzmann equation that exhibits the same form as the one for a monatomic gas [31]. The moment technique can be applied successfully to this equation, deriving a double infinite hierarchy of balance laws, which involve two species of moments [15]

$$\begin{aligned}
&\partial_t F+\partial_j F_j=0,\\
&\qquad\swarrow\\
&\partial_t F_{i_1}+\partial_j F_{ji_1}=0,\\
&\qquad\swarrow\\
&\partial_t F_{i_1i_2}+\partial_j F_{ji_1i_2}=P_{i_1i_2},\quad \partial_t G_{ss}+\partial_j G_{ssj}=0,\\
&\qquad\swarrow\qquad\qquad\swarrow\\
&\partial_t F_{i_1i_2i_3}+\partial_j F_{ji_1i_2i_3}=P_{i_1i_2i_3},\quad \partial_t G_{ssi_1}+\partial_j G_{ssji_1}=Q_{ssi_1},\\
&\vdots\qquad\qquad\qquad\qquad\vdots\\
&\partial_t F_{i_1i_2\ldots i_h}+\partial_j F_{ji_1i_2\ldots i_h}=P_{i_1i_2\ldots i_h},\quad \partial_t G_{ssi_1i_2\ldots i_h}+\partial_j G_{ssji_1i_2\ldots i_h}=Q_{ssi_1i_2\ldots i_h}.\\
&\vdots\qquad\qquad\qquad\qquad\vdots
\end{aligned}\tag{2.1}$$

where $\partial_t\cdot=\partial\cdot/\partial t$ and $\partial_j\cdot=\partial\cdot/\partial z_j$ with $j=1,2,3$, while the so-called momentum-like F moments and the energy-like G moments are defined as

$$F=m\int_{\mathbb{R}^3}\int_0^{+\infty} f\varphi(I)dI\,d\mathbf{c},\quad F_{i_1i_2\ldots i_h}=m\int_{\mathbb{R}^3}\int_0^{+\infty} fc_{i_1}c_{i_2}\ldots c_{i_h}\varphi(I)dId\mathbf{c}$$

and

$$G_{ss}=m\int_{\mathbb{R}^3}\int_0^{+\infty} f\left(c^2+\frac{2I}{m}\right)\varphi(I)dId\mathbf{c},$$

$$G_{ssi_1\ldots i_h}=m\int_{\mathbb{R}^3}\int_0^{+\infty} f\left(c^2+\frac{2I}{m}\right)c_{i_1}c_{i_2}\ldots c_{i_h}\varphi(I)dId\mathbf{c},$$

if $h\in\mathbb{N}\backslash\{0\}$, $i_h=1,2,3$ and m denotes the mass of the gas molecule. The weighting measure $\varphi(I)$ is prescribed in order to set the equilibrium caloric equation of state for a polyatomic gas [15]. For a polytropic gas, the internal energy at equilibrium is given by $\varepsilon=Dk_BT/(2m)$ (if k_B denotes the Boltzmann constant, T the temperature and D the degrees of freedom of a gas molecule) and

royalsocietypublishing.org/journal/rspa Proc. R. Soc. A 478: 20220246

it was proved that $\varphi(I) = I^a$ with $a = (D-5)/2$. In (2.1), $P_{i_1 \dots i_h}$ and $Q_{ssi_1 \dots i_h}$ are the productions derived from the collisional term of the Boltzmann equation, through the moment technique. Moreover, from now on repeated indexes imply their sum, so that for example $\sum_{j=1}^{3}$ is omitted in (2.1).

We recall that the first two equations of the momentum-hierarchy and the first scalar equation of the energy-hierarchy coincide with the usual conservation laws of mass, momentum and energy. In both hierarchies (2.1), it is also evident that the density component of one equation coincides with the flux component of the previous one. The infinite set of PDEs (2.1) is then truncated at some truncation indexes (N for the F-hierarchy and M for the G-hierarchy) and the maximum entropy principle (MEP) is commonly employed in order to establish how to express the last fluxes and production terms as functions of the independent field variables. Appendix A contains a brief presentation of the truncation procedure and of the construction of an RET theory with 14 moments, for more details, see [15]. The resulting equation system turns out to be of hyperbolic type, and for a convenient choice of the independent field variables (*main field* [32,33]), it could be written in a symmetric hyperbolic form with a convex entropy, so that the well-posedness of the Cauchy problem is guaranteed.

As in the case of monatomic gases, the moments truncated through the previous procedure are usually approximated by a Taylor expansion in the neighbourhood of a local equilibrium. In the present paper, we will focus on a linearized theory with respect to the non-equilibrium variables (see appendix A for more details), usually [15] denoted by $\mathrm{ET}^1_{n,P}$, where the '1' represents the first order approximation, n is the number of scalar equations of the model and P indicates the fact that we are dealing with a polyatomic gas. A vectorial concise notation frequently adopted in RET indicates the density, the flux and the productions components as

$$\begin{aligned}
&\mathbf{F} = (F, F_{i_1}, F_{i_1 i_2}, \dots F_{i_1 i_2 \dots i_N})^T, \quad \mathbf{F}^j = (F_j, F_{ji_1}, F_{ji_1 i_2}, \dots F_{ji_1 i_2 \dots i_N})^T,\\
&\mathbf{G}_{ss} = (G_{ss}, G_{ssi_1}, G_{ssi_1 i_2}, \dots G_{ssi_1 i_2 \dots i_M})^T,\\
&\mathbf{G}^j_{ss} = (G_{ssj}, G_{ssji_1}, G_{ssji_1 i_2}, \dots G_{ssji_1 i_2 \dots i_M})^T,\\
&\mathbf{P} = (0, 0_{i_1}, P_{i_1 i_2}, \dots P_{i_1 i_2 \dots i_N})^T, \quad \mathbf{Q} = (0, Q_{ssi_1}, Q_{ssi_1 i_2}, \dots Q_{ssi_1 i_2 \dots i_M}),
\end{aligned}$$

so that the closed truncated PDE system can be briefly written as

$$\partial_t \mathbf{F} + \partial_j \mathbf{F}^j = \mathbf{P} \quad \text{and} \quad \partial_t \mathbf{G}_{ss} + \partial_j \mathbf{G}^j_{ss} = \mathbf{Q}. \tag{2.2}$$

In what follows, we will analyse wave phenomena depending on a unique scalar space variable, denoted by $z = z_1$. In this case, if $\mathbf{u}$ indicates the vector of the field variables, system (2.2) can be further rewritten as

$$\mathbf{C(u)}\, \partial_t \mathbf{u} + \mathbf{D(u)}\, \partial_z \mathbf{u} = \mathbf{T}', \quad \text{with } \mathbf{C(u)} = \partial_{\mathbf{u}}(\mathbf{F}, \mathbf{G}_{ss}),\ \mathbf{D(u)} = \partial_{\mathbf{u}}(\mathbf{F}^1, \mathbf{G}^1_{ss}), \tag{2.3}$$

if $\mathbf{T}' = (\mathbf{P}, \mathbf{Q})$ and $\partial_z = \partial \cdot / \partial z$. One refers commonly to the material derivative $\overset{\bullet}{*} = \partial * / \partial t + v(\partial * / \partial z)$, where v is the gas velocity along the z-direction, and thanks to the hyperbolcity properties it is possible to write down (2.3) as

$$\partial_t \mathbf{u} + \mathbf{A(u)} \partial_z \mathbf{u} = \mathbf{T} \Longrightarrow \overset{\bullet}{\mathbf{u}} + \mathbf{B(u)} \partial_z \mathbf{u} = \mathbf{T}, \tag{2.4}$$

where $\mathbf{A} = \mathbf{C}^{-1}\mathbf{D}$, $\mathbf{T} = \mathbf{C}^{-1}\mathbf{T}'$ and $\mathbf{B} = \mathbf{A} - v\mathbf{I}$, if $\mathbf{I}$ denotes an identity matrix of the same size as the square matrix $\mathbf{A}$. The characteristic velocities associated with the equation system can be determined looking for the eigenvalues λ of $\mathbf{A}$, and obviously the eigenvalues Λ of $\mathbf{B}$ and those of $\mathbf{A}$ satisfy the relation $\lambda = \Lambda + v$. To determine the behaviour of the AWs, we will consider both the characteristic velocities and the right and left eigenvectors associated with $\mathbf{A}$.

For the sake of simplicity, here we will restrict our analysis to ideal polyatomic gases, which present specific heat at constant volume $c_v = k_B D/2m$, D can be seen as the sum of translational and internal degrees of freedom and it must hold $D \geq 3$, where $D = 3$ corresponds to monatomic molecules.

One of the most popular theories derived through the RET procedures is the 14-moment system $\mathrm{ET}^1_{14,P}$, in which together with mass density ρ, velocity $\mathbf{v}=(v_1,v_2,v_3)$ and equilibrium pressure p, also the deviatoric part of the viscous stress tensor $\sigma_{\langle ij\rangle}$, the dynamic pressure Π and the heat flux $\mathbf{q}=(q_1,q_2,q_3)$ are treated as independent field variables, so that

$$\mathbf{F}=(F,F_k,F_{kl}),\quad \mathbf{F}^j=(F_j,F_{jk},F_{jkl}),\ \mathbf{G}_{ss}=(G_{ss},G_{ssk}),\ \mathbf{G}^j_{ss}=(G_{ssj},G_{ssjk})$$

with $F=\rho$, $F_k=\rho v_k$, $F_{kl}=\rho v_k v_l+(p+\Pi)\delta_{kl}-\sigma_{\langle kl\rangle}$,

$$\begin{aligned}
F_{jkl}&=\rho v_j v_k v_l+(p+\Pi)(v_j\delta_{kl}+v_k\delta_{jl}+v_l\delta_{jk})-\sigma_{\langle jk\rangle}v_l-\sigma_{\langle kl\rangle}v_j-\sigma_{\langle jl\rangle}v_k\\
&\quad+\frac{2}{D+2}(q_j\delta_{kl}+q_k\delta_{jl}+q_l\delta_{jk}),\\
G_{ss}&=\rho|v|^2+2\rho\epsilon,\quad G_{ssk}=\rho|v|^2v_k+2(\rho\epsilon+p+\Pi)v_k-2\sigma_{\langle ks\rangle}v_s+2q_k,\\
G_{ssjk}&=\rho|v|^2v_jv_k+2\rho\epsilon v_jv_k+(p+\Pi)(|v|^2\delta_{jk}+4v_jv_k)-\sigma_{\langle jk\rangle}|v|^2-2\sigma_{\langle jh\rangle}v_kv_h\\
&\quad-2\sigma_{\langle kh\rangle}v_jv_h+\frac{2}{D+2}(2q_hv_h\delta_{jk}+(D+4)(q_jv_k+q_kv_j))\\
&\quad+\frac{k_BT}{m}[(D+2)p+(D+4)\Pi]\delta_{jk}-\frac{k_BT}{m}(D+4)\sigma_{\langle jk\rangle},\quad \text{if } i,j,k,l,s=1,2,3.
\end{aligned}\tag{2.5}$$

The monatomic RET theory with 13 moments (the well-known Grad's one) can be derived from $\mathrm{ET}^1_{14,P}$ in the limit $D\to 3$, neglecting the dynamic pressure, which does not play any role in monatomic gases. Concerning the notation, we will denote Grad's system by ET^1_{13} in order to recall that it is a first-order theory in the non-equilibrium variables with 13 moments and it is valid for a monatomic gas.

(a) Rational extended thermodynamics balance laws in different geometries

In the next sections, we are going to study planar, cylindrical and spherical AWs. In order to describe their wave fronts through a one-dimensional space set of balance laws, it is convenient to pass from Cartesian to curvilinear coordinates when a cylindrical or spherical geometry is involved. Thus, together with the usual rectangular Cartesian coordinates (x_1,x_2,x_3), we will refer to cylindrical coordinates (r,ϑ,x_3) ($\vartheta\in[0,2\pi[$) and spherical coordinates (r,ϑ,φ) ($\vartheta\in[0,2\pi[$ and $\varphi\in[0,\pi]$). In the following, instead of the usual contra- or co-variant components of vectors and tensors, we will employ the physical components [34,35], so that, for example

$$\bar{q}^i=\sqrt{g_{\underline{i}\underline{i}}}q^i,\quad \bar{\sigma}^{\langle ij\rangle}=\sqrt{g_{\underline{i}\underline{i}}g_{\underline{j}\underline{j}}}\sigma^{\langle ij\rangle},\ \text{with } i,j,=1,2,3,$$

where the repeated underlined indexes are not summed and g_{ij} represents the (ij) component of the metric tensor.[1] The bar denotes here the physical component, but in the following, we will omit such a symbol for the sake of brevity. We preliminarily assume that the heat flux and the gas velocity are parallel to the first component of the Cartesian space variables in the planar geometry or they are parallel to the radial direction in the remaining cases. Hence, we impose that

$$\mathbf{v}=(v,0,0)\quad\text{and}\quad\mathbf{q}=(q,0,0),\ \text{with } v=v^1,\ q=q^1,$$

and, moreover,

$$\sigma^{\langle ij\rangle}=0\quad\text{when } i\neq j.$$

We recall that, by definition, $\sigma^{\langle ll\rangle}=0$. In planar or spherical geometry, this last relation and a reasonable assumption of space homogeneity imply that $\sigma^{\langle 22\rangle}=\sigma^{\langle 33\rangle}=-\sigma^{\langle 11\rangle}/2$, but this condition cannot be prescribed in cylindrical symmetry. Thus, in the following set of balance laws, we have to include also the equation for $\sigma^{\langle 22\rangle}$. We write it in the last row, since it can be omitted for planar or spherical AWs. In order to compact in a single set of equations the cases

[1]In cylindrical geometry, the metric tensor turns out to be diagonal with $g_{11}=g_{33}=1$, $g_{22}=r^2$, while in the spherical case the non-vanishing components of the diagonal metric tensor are $g_{11}=1$, $g_{22}=r^2\sin^2\vartheta$, $g_{33}=r^2$.

corresponding to different geometries, we introduce the parameter g with the following usual convention: $g=0$ corresponds to the planar case, $g=1$ the cylindrical case, while for spherical symmetry $g=2$. Thus, the field equations become

$$\begin{aligned}
&\dot{\rho}+\rho\,\partial_z v=P_1,\\
&\dot{v}-\frac{1}{\rho}\partial_z\sigma^{\langle 11\rangle}+\frac{1}{\rho}\partial_z\Pi+\frac{1}{\rho}\partial_z p=P_2,\\
&\dot{\sigma}^{\langle 11\rangle}+\frac{7\sigma^{\langle 11\rangle}-4(p+\Pi)}{3}\partial_z v-\frac{8}{3(D+2)}\partial_z q=P_3,\\
&\dot{\Pi}+[\Pi-\frac{2(D-3)(\sigma^{11}-p)}{3D}]\partial_z v+\frac{4(D-3)}{3D(D+2)}\partial_z q=P_4,\\
&\dot{p}+[p+\frac{2(p-\sigma^{11})}{D}]\partial_z v+\frac{2}{D}\partial_z q=P_5,\\
&\dot{q}+\frac{p}{2\rho^2}[2\sigma^{11}-(D+2)(p-\sigma^{11})]\partial_z\rho+\frac{2(D+5)q}{D+2}\partial_z v-\frac{\sigma^{11}+p}{\rho}(\partial_z\sigma^{\langle 11\rangle}-\partial_z\Pi)\\
&\quad+\frac{(D+2)(p-\sigma^{11})}{2\rho}\partial_z p=P_6,\\
&\dot{\sigma}^{\langle 22\rangle}+\left[\frac{2}{3}(p+\Pi-\sigma^{\langle 11\rangle})+\sigma^{\langle 22\rangle}\right]\partial_z v+\frac{4}{3(D+2)}\partial_z q=P_7,
\end{aligned}\tag{2.6}$$

where

$$\begin{aligned}
&P_1=-g\frac{\rho v}{z},\quad P_2=g\frac{(\sigma^{\langle 11\rangle}-\sigma^{\langle 22\rangle})}{z\rho},\ P_5=-2g\frac{q}{Dz}-2g\frac{(p+\Pi-\sigma^{\langle 22\rangle})v}{Dz}-g\frac{pv}{z},\\
&P_3=-\frac{\sigma^{\langle 11\rangle}}{\tau_\sigma}-\frac{4gq}{3(D+2)z}-\frac{gv}{3z}[2(p+\Pi+\sigma^{\langle 11\rangle}-2\sigma^{\langle 22\rangle})+g(\sigma^{\langle 11\rangle}+2\sigma^{\langle 22\rangle})],\\
&P_4=-\frac{\Pi}{\tau_\Pi}-g\frac{4(D-3)q}{3D(D+2)z}\\
&\quad-g\frac{6(\sigma^{\langle 22\rangle}-p-\Pi)+D(-\sigma^{\langle 11\rangle}-4\sigma^{\langle 22\rangle}+5\Pi+2p+g(\sigma^{\langle 11\rangle}+2\sigma^{\langle 22\rangle}))v}{3Dz},\\
&P_6=-\frac{q}{\tau_q}-\frac{g}{z}\left[\frac{(\sigma^{\langle 22\rangle}-\sigma^{\langle 11\rangle})(p+\sigma^{11})}{\rho}+\frac{(D+4)qv}{D+2}\right],\\
&P_7=-\frac{\sigma^{\langle 22\rangle}}{\tau_\sigma}-g\frac{2(3g-7)q}{3(D+2)z}-\frac{gv}{3z}[8\sigma^{\langle 22\rangle}-\sigma^{\langle 11\rangle}-7p-7\Pi+g(3p+3\Pi+\sigma^{\langle 11\rangle}-\sigma^{\langle 22\rangle})],
\end{aligned}\tag{2.7}$$

if τ_Π, τ_σ and τ_q represent the relaxation times of dynamic pressure, stress tensor and heat flux, related, respectively, to the bulk viscosity ν, the shear viscosity μ_v and the heat conductivity κ of the gas [15,16] by

$$\tau_\sigma=\frac{\mu_v}{p},\quad \tau_q=\frac{2\kappa m}{5k_B p},\quad \tau_\Pi=\frac{3D\nu}{2(D-3)p}.\tag{2.8}$$

Moreover, the (11)-component of the viscous tensor $\sigma^{11}=\sigma^{\langle 11\rangle}-\Pi$ was introduced in (2.6) and (2.7) to compress some expressions. We remark that only the production terms depend on the AW geometry, while the PDEs structure remains unvaried when the parameter g is changed.

3. A brief presentation of the theory of acceleration waves

As recalled in the introduction, an AW indicates a propagating surface Γ across which all the field variables are continuous, differently from the first derivatives of at least one field variable that exhibit a jump. In particular, the derivative of the velocity could present a jump, hence the name AW. The wavefront Γ can be seen as a surface that separates the space into two subspaces:

in the subspace ahead the front the unperturbed field variables are known functions $\mathbf{u}_u(\mathbf{z},t)$ of the space and time variables $\mathbf{z}$ and t, while behind Γ the perturbed field variables $\mathbf{u}(\mathbf{z},t)$ are usually unknown. If $\varphi(\mathbf{z},t)=0$ represents the equation of the wavefront and the jump across Γ is denoted by $[\![\cdot]\!]=(\cdot)_{\varphi=0^-}-(\cdot)_{\varphi=0^+}$, the peculiarities of an AW are easily summarized as $[\![\mathbf{u}]\!]=\mathbf{0}$ and $[\![\partial\mathbf{u}/\partial\varphi]\!]=\mathcal{A}\neq\mathbf{0}$.

As already mentioned, in the present paper, we will restrict our attention to planar weak discontinuities and to cylindrical and spherical ones, which propagate along the radial direction. Thanks to a suitable change in space coordinates it will always be possible to reduce the problem to a one-dimensional study of AWs. In this manner, the field variables and the equation of the wavefront will depend only on z (that plays the role of the first Cartesian coordinate for a planar wave or the radial variable for cylindrical/spherical waves). For a one-dimensional weak discontinuity, the well-established theory of AW [1–3] states that

— The normal velocity $v=-\varphi_t/|\nabla\varphi|$ of the wavefront coincides with the characteristic speed of the hyperbolic PDE system evaluated in the unperturbed field $V=\lambda(\mathbf{u}_u)$.
— The jump vector $\mathcal{A}$ is proportional to the right eigenvectors corresponding to λ, evaluated in $\mathbf{u}_u$, so that $\mathcal{A}=\mathcal{A}\mathbf{r}(\mathbf{u}_u)$.
— The scalar amplitude $\mathcal{A}$ satisfies the Bernoulli equation

$$\frac{\mathrm{d}\mathcal{A}}{\mathrm{d}t}+a(t)\mathcal{A}^2+b(t)\mathcal{A}=0, \tag{3.1}$$

if d/dt indicates the time derivative along the characteristic line ($\mathrm{d}x/\mathrm{d}t=\lambda(\mathbf{u}_u)$) and $a(t)$ and $b(t)$ are suitable function of time.

In this way, the time dependence of the scalar amplitude is easily deduced if $\mathcal{A}(0)$ represents the initial value of the scalar amplitude at time $t=0$

$$\mathcal{A}(t)=\frac{\mathcal{A}(0)g_1(t)}{1+\mathcal{A}(0)g_2(t)} \text{ with } g_1(t)=\exp\left(-\int_0^t b(s)\,\mathrm{d}s\right) \quad \text{and} \quad g_2(t)=\int_0^t a(s)g_1(s)\,\mathrm{d}s. \tag{3.2}$$

Concerning the calculation of Bernoulli's coefficients a and b, for one-dimensional waves and for a set of PDEs written as

$$\partial_t\mathbf{u}+\mathbf{A}(\mathbf{u},z,t)\partial_z\mathbf{u}=\mathbf{T}(\mathbf{u},z,t), \tag{3.3}$$

in [3] it is shown that

$$\left.\begin{aligned} a(t)&=\varphi_z(t)(\nabla_{\mathbf{u}}\lambda\cdot\mathbf{r})\Big|_u \\ \text{and}\qquad b(t)&=\left\{\mathbf{r}((\nabla_{\mathbf{u}}\mathbf{l})^T-\nabla_{\mathbf{u}}\mathbf{l})\cdot\frac{\mathrm{d}\mathbf{u}}{\mathrm{d}t}+(\nabla_{\mathbf{u}}\lambda\cdot\mathbf{r})(\mathbf{l}\cdot\mathbf{u}_z)-\nabla_{\mathbf{u}}(\mathbf{l}\cdot\mathbf{T})\cdot\mathbf{r}+\mathbf{l}\cdot\frac{\tilde{\mathrm{d}}\mathbf{r}}{\mathrm{d}t}\right\}\Big|_u, \end{aligned}\right\} \tag{3.4}$$

if $w_z=\partial w/\partial z$ for any w and $\nabla_{\mathbf{u}}\cdot=\partial\cdot/\partial\mathbf{u}$. In addition, $\mathbf{l}(\mathbf{u},z,t)$ and $\mathbf{r}(\mathbf{u},z,t)$ denote respectively the left and right eigenvector of $\mathbf{A}$ associated with the eigenvalue λ. For any function w of the field variables we refer to the notation: $w|_u=w(\mathbf{u}_u)$, while $\mathrm{d}\cdot/\mathrm{d}t=\partial_t\cdot+\lambda_u\partial_{z^1}\cdot$ and $\tilde{\mathrm{d}}\cdot/\mathrm{d}t=(\mathrm{d}\cdot/\mathrm{d}t)|_{\mathbf{u}=\text{const}}$.

A brief comment should be added to the choice of the left and right eigenvectors, since in principle they are both defined apart from an arbitrary factor. In what follows, we prescribe the arbitrary factor of $\mathbf{l}$ requiring that $\mathbf{l}\cdot\mathbf{r}=1$ (this requirement is necessary to make valid the previous points), while we can imagine that the arbitrary factor of the right eigenvector is absorbed by the scalar amplitude $\mathcal{A}$. However, for an AW propagating with a non-vanishing $\lambda_u=\lambda(\mathbf{u}_u)$ velocity, the arbitrary factor can be fixed referring to the Hadamard relation, obtaining the time evolution equation for the acceleration jump $\mathcal{G}$. In all the cases analysed in the present

work the second component of $\mathbf{u}$ turns out to be the gas velocity v along the z-direction, so that $[\![\partial v/\partial z]\!] = \mathcal{A}_2 = \mathcal{A}r_2$ and thanks to the Hadamard condition it must hold

$$\mathcal{G} = \left[\!\left[\frac{\partial v}{\partial t} \right]\!\right] = -\lambda_u \left[\!\left[\frac{\partial v}{\partial z^1} \right]\!\right] = -\lambda_u \mathcal{A} r_2(\mathbf{u}_u), \quad \text{hence } \mathcal{G} = \mathcal{A} \Longleftrightarrow r_2(\mathbf{u}_u) = -\frac{1}{\lambda_u}.$$

Imposing this condition, the scalar amplitude $\mathcal{A}$ always coincides with $\mathcal{G}$. The study of AWs is often restricted to the fastest one. As a matter of fact, a hyperbolic system presents frequently different characteristic velocities and consequently different AWs that propagate with various speeds. So, if some waves are simultaneously present, only the fastest wave propagates into the unperturbed solution $\mathbf{u} = \mathbf{u}_u$.

Concerning the time dependence of $\mathcal{A}$, it is well known [1–3] that for an AW that satisfies the condition $\partial\lambda/\partial\mathbf{u} \cdot \mathbf{r} \neq 0$ and for any suitable initial values $|\mathcal{A}(0)| > |\mathcal{A}_{\rm cr}|$, there exists a critical time $t_{\rm cr}$ such that the solution diverges, due to the annulment of the denominator in (3.2): $1 + \mathcal{A}(0) g_2(t_{\rm cr}) = 0$. Under this condition, the AW degenerates into a shock wave and the field variables present jumps across Γ. Thanks to the monotonicity of g_2, it is possible to prove that $\mathcal{A}_{\rm cr} = -\lim_{t\to\infty} 1/g_2(t)$.

As a final remark, we stress that the shock formation can be seen as a nonlinear stability problem for the unperturbed field $\mathbf{u}_u$, as it was observed in [3]. In particular, the regular solution $\mathbf{u}_u$ is λ-*stable* if there exist suitable initial perturbation values $\mathcal{A}(0)$ such that $\mathcal{A}(t)$ exists for any $t \geq 0$ and it is bounded.

4. Acceleration waves in a polyatomic gas described by $\mathrm{ET}^1_{14,P}$

To study the AWs predicted by $\mathrm{ET}^1_{14,P}$, we will follow the procedure described in §3, starting from the characteristic polynomial, the characteristic velocities and the corresponding left and right eigenvectors. Then, referring to (3.4), we determine analytically the coefficients of Bernoulli's equation (3.1), and the functions g_1 and g_2 from (3.2).

The characteristic velocities ($\lambda = \Lambda + v$) associated with system (2.6) are easily calculated [15] looking for the roots of the corresponding characteristic polynomial

$$\begin{aligned}
&\mathcal{P}(\Lambda) = 0 \Longleftrightarrow \Lambda^3(p_4\Lambda^4 + p_2\Lambda^2 + p_1\Lambda + p_0) = 0\\
&\text{if } p_4 = D(D+2)^2\rho^2, \quad p_2 = -2(D+2)\rho(-(4+3D+2D^2)\sigma^{11} + (7D+2D^2)p),\\
&p_1 = -12D(D+5)q\rho, \quad p_0 = 3D(D+2)((4+D)\sigma^{11}{}^2 - (4+2D)\sigma^{11}p + (D+2)p^2).
\end{aligned}$$

We take into account the unperturbed solution of a gas at rest and at equilibrium ($v_u = 0$, $\Pi_u = \sigma_u^{\langle 11\rangle} = \sigma_u^{\langle 22\rangle} = 0$, $q_u = 0$, $\rho_u = \rho_0$, $p_u = p_0$), so that the velocities of the AWs propagating in the unperturbed field $\lambda_u = \lambda|_u = \Lambda|_u$ are given by

$$\lambda_{1,2}|_u = \pm\sqrt{\frac{L_1 + \sqrt{L_2}}{D+2}}\sqrt{\frac{p_0}{\rho_0}}, \quad \lambda_{3,4}|_u = \pm\sqrt{\frac{L_1 - \sqrt{L_2}}{D+2}}\sqrt{\frac{p_0}{\rho_0}}, \ \lambda_{5,6,7}|_u = 0,$$

with $L_1 = 2D + 7$ and $L_2 = D^2 + 16D + 37$. In what follows, we restrict our attention to non-exceptional AWs propagating with non-zero velocity. We stress that the wave speed does not depend on the wave front geometry, but rather on the degrees of freedom of the gas molecule. The left and right eigenvectors associated with λ present a quite complicated structure and for

the sake of simplicity, we report here only the expression of the right eigenvector when $\mathbf{u} = \mathbf{u}_u$ (see §3):

$$\mathbf{r}|_u = (r_1, r_2, r_3, r_4, r_5, r_6, r_7), \quad \text{if } r_2 = -\frac{1}{\lambda_u},\ r_d = -(D+2)\lambda_u^2\rho_0 + (D+8)p_0,$$
$$r_1 = r_2\frac{\rho_0}{\lambda_u},\ r_3 = \frac{r_2}{3r_d\lambda_u}(4(D+2)p_0(p_0 - \lambda_u^2\rho_0)),$$
$$r_4 = -\frac{r_2}{3Dr_d\lambda_u}2(D-3)(D+2)p_0(p_0 - \lambda_u^2\rho_0),$$
$$r_5 = -\frac{r_2}{Dr_d\lambda_u}(D+2)^2p_0(p_0 - \lambda_u^2\rho_0),$$
$$r_6 = \frac{r_2}{r_d}3(D+2)p_0^2,\ r_7 = -\frac{r_2}{3r_d\lambda_u}2(D+2)p_0(p_0 - \lambda_u^2\rho_0).$$

The equation of the wave front is determined recalling that λ_u is constant and imposing that the AW front starts at $z(t=0) = z_0$

$$\overset{\bullet}{\varphi} = \partial_t\varphi + \lambda_u\partial_z\varphi = 0 \Rightarrow \varphi(t,z) = z - z_0 - \lambda_u t = 0 \Rightarrow z(t) = z_0 + \lambda_u t. \tag{4.1}$$

Since the AW propagates in an unperturbed constant state where the gas is in equilibrium and at rest, all the production terms in (2.6) vanish and the coefficients a and b are easily deduced by (3.4)

$$a = \frac{3(D+2)p_0^2(a_1\lambda_u^2\rho_0 - a_2p_0)}{D^2\lambda_u^3\rho_0 r_d((D+2)\lambda_u^2\rho_0 - (2D-7)p_0)},$$
$$b = b(t) = \frac{b_\sigma}{\tau_\sigma} + \frac{b_\Pi}{\tau_\Pi} + \frac{b_q}{\tau_q} + b_g\frac{g}{z(t)} = \beta + b_g\frac{g}{z(t)},$$
$$a_1 = (D+2)(2D^2+11D-4), \quad a_2 = (2D^3+3D^2+8D-4), \tag{4.2}$$
$$b_g = \frac{\lambda_u}{2}, \quad b_\sigma = \frac{(D+2)(\lambda_u^2\rho_0 - p_0)^2}{9p_0((D+5)\lambda_u^2\rho_0 - (D-1)p_0)},$$
$$b_\Pi = \frac{(D-3)}{2D}b_\sigma,\ b_q = \frac{27\lambda_u^2p_0\rho_0}{2(D+2)(\lambda_u^2\rho_0 - p_0)^2}b_\sigma,$$

where $z(t)$ indicates the position of the AW front at instant t, determined in (4.1). We remark that coefficient a is constant, regardless of the value of g; additionally, its expression includes the monatomic case as a limit case when $D \to 3$. A comparison of a with calculations for monatomic gases in [8,9] is not immediate, since there the right and left eigenvectors were differently normalized. On the contrary, when $D = 3$ and planar geometry is taken into account ($g = 0$) the expression of b coincides with the monatomic one derived in [8,9]. It is evident that coefficient b contains terms that account for the AW geometry, as already observed by Lindsay & Straughan [5] for a different model.

The calculation of $g_1(t)$ and $g_2(t)$ from (3.2) and (4.2) is carried out, recalling that $(b_g g/z(t) = (g/2)(\mathrm{d}\ln(z(t))/\mathrm{d}t)$ (see (4.1)). The final expression of the integral functions can be summarized as

$$\text{if } g = 0 \text{ and } \alpha \lessgtr 0 \quad g_1(t) = \exp(-\beta t),\ g_2(t) = \frac{a}{\beta}(1 - \exp(-\beta t)),$$
$$\text{if } g = 1 \text{ and } \alpha > 0 \quad g_1(t) = \frac{\mathrm{e}^{-\beta t}}{\sqrt{1+\alpha t}},\ g_2(t) = a\sqrt{\pi}\frac{\mathrm{e}^{\beta/\alpha}}{\sqrt{\alpha\beta}}\Delta\mathrm{erf}(\beta,\alpha,t),$$
$$\text{if } g = 1 \text{ and } \alpha < 0 \quad g_1(t) = \frac{\mathrm{e}^{-\beta t}}{\sqrt{1+\alpha t}},\ g_2(t) = -a\sqrt{\pi}\frac{\mathrm{e}^{\beta/\alpha}}{\sqrt{-\alpha\beta}}\Delta\mathrm{erfi}(\beta,\alpha,t),$$
$$\text{if } g = 2 \text{ and } \alpha \lessgtr 0 \quad g_1(t) = \frac{\mathrm{e}^{-\beta t}}{1+\alpha t},\ g_2(t) = \frac{a}{\alpha}\mathrm{e}^{\beta/\alpha}\Delta\mathrm{Ei}(\beta,\alpha,t),$$

if $\alpha = \lambda_u/z_0$ ($\alpha > 0$ for an outgoing AW, while $\alpha < 0$ for an incoming AW), and Δerf, Δerfi and ΔEi denote suitable differences of the well-known integral functions,

$$\Delta\mathrm{erf}(\beta,\alpha,t) = \mathrm{erf}\left(\sqrt{\frac{\beta(1+\alpha t)}{\alpha}}\right) - \mathrm{erf}\left(\sqrt{\frac{\beta}{\alpha}}\right), \quad \text{if } \mathrm{erf}(w) = \frac{2}{\sqrt{\pi}}\int_0^w \mathrm{e}^{-s^2}\,\mathrm{d}s,$$

$$\Delta\mathrm{erfi}(\beta,\alpha,t) = \mathrm{erfi}\left(\sqrt{\frac{\beta(1+\alpha t)}{-\alpha}}\right) - \mathrm{erfi}\left(\sqrt{\frac{\beta}{-\alpha}}\right), \quad \text{if } \mathrm{erfi}(w) = \frac{2}{\sqrt{\pi}}\int_0^w \mathrm{e}^{s^2}\,\mathrm{d}s,$$

$$\Delta\mathrm{Ei}(\beta,\alpha,t) = \mathrm{Ei}\left(-\frac{\beta}{\alpha}(1+\alpha t)\right) - \mathrm{Ei}\left(-\frac{\beta}{\alpha}\right), \quad \text{if } \mathrm{Ei}(w) = -\int_{-w}^{\infty}\frac{\mathrm{e}^{-s}}{s}\,\mathrm{d}s.$$

As already stated in §3, non-exceptional AWs present critical times t_{cr}, which satisfy the equation $1 + \mathcal{A}(0)g_2(t_{\mathrm{cr}}) = 0$. A necessary condition for shock formation is related to the sign of $\mathcal{A}(0)$ that should be concordant with that of the characteristic velocity. Moreover, taking into account the previous table, it is easily verified that only in the planar case critical time and critical amplitude can be determined explicitly as $t_{\mathrm{cr}} = -(1/\beta)\ln(1 + (\beta/a\mathcal{A}(0)))$, and $\mathcal{A}_{\mathrm{cr}} = -\beta/a$.

If $g = 1, 2$, the analytic calculation of both t_{cr} and $\mathcal{A}_{\mathrm{cr}}$ is no longer possible, although such values undoubtedly exist due to the monotonicity of functions $g_2(t)$. In such cases, the numerical evaluation was performed by MATLAB.

For outgoing AWs (i.e. $\alpha > 0$), it is rigorously shown that $\mathcal{A}_{\mathrm{cr}}|_{g=2} \geq \mathcal{A}_{\mathrm{cr}}|_{g=1} \geq \mathcal{A}_{\mathrm{cr}}|_{g=0}$ and that in the limit $(\beta/\alpha) \to \infty$ the critical amplitude in spherical and cylindrical geometry converges to the planar one.[2] Thus, we conclude that a radial geometry has a stabilizing effect on the AW behaviour.

In figure 1*a*, we present a qualitative sketch of $\mathcal{A}(t)$ behaviour as its initial value $\mathcal{A}(0)$ changes. Figure 1 on the right shows a comparison of $\mathcal{A}_{\mathrm{cr}}$ as a function of D and for different wave geometries. The plots focus on the fastest AW and are obtained assuming the same value of temperature, molecular mass and relaxation times for any value of D ($T = 300\,\mathrm{K}$, $m = 66.4 \times 10^{-27}\,\mathrm{Kg}$, $\tau_\sigma = \tau_q = \tau_\Pi = 10^{-8}\mathrm{s}$) and fixing $r_0 = 4 \times 10^{-5}\,\mathrm{m}$. These unrealistic hypotheses were introduced in order to highlight the role played by the geometry and by D in the determination of critical amplitude values. When $r_0 \geq 1\,\mathrm{mm}$ (i.e. more realistic physical situations) the value of $\mathcal{A}_{\mathrm{cr}}$ in radial geometry converges to the corresponding one of a planar AW within the plot precision. We stress that in all the cases $\mathcal{A}_{\mathrm{cr}}$ exceeds by some orders of magnitude a realistic physical value of the initial scalar amplitude, making shock formation very unlikely. Moreover, the dependence on D is not particularly pronounced and the minimum of $\mathcal{A}_{\mathrm{cr}}$ is observable for monatomic gases ($D = 3$).

A final remark concerns the spherical or cylindrical incoming wave front $z(t)$, which converges to the centre after a time $-1/\alpha$. Consequently, function $g_1(t)$ diverges for any initial scalar amplitude in radial geometry. Surprisingly, in the spherical case also the term $\Delta Ei(\beta,\alpha,t)$ contained in g_2 diverges when $t \to -1/\alpha$ (see (4.1)). This peculiarity was already observed for a different model by Lindsay & Straughan [5] and it was noted for an Euler gas in the special case of bubble dynamics by Greenspan & Nadim [17]. In other words, $\forall\ \mathcal{A}(0) < 0$ a spherical AW with negative velocity becomes a shock wave in a sufficiently small neighbourhood of the sphere centre. This case will be the subject of the second part of the present work.

5. Rational extended thermodynamics in an oscillating bubble

In the previous sections, we studied physical systems that exhibit similar behaviours in the presence of monatomic or polyatomic gases. Now, we are looking for a physical framework in which differences between such gases can be observed experimentally and suitable for the study of AWs. To this end, in what follows, we will consider gas bubbles oscillating within a liquid, due to the presence of an external sound field. The bubble is commonly supposed to maintain a perfect

[2]The proof follows from the comparison of the integrand functions in $(3.2)_3$ for planar, cylindrical and spherical geometry.

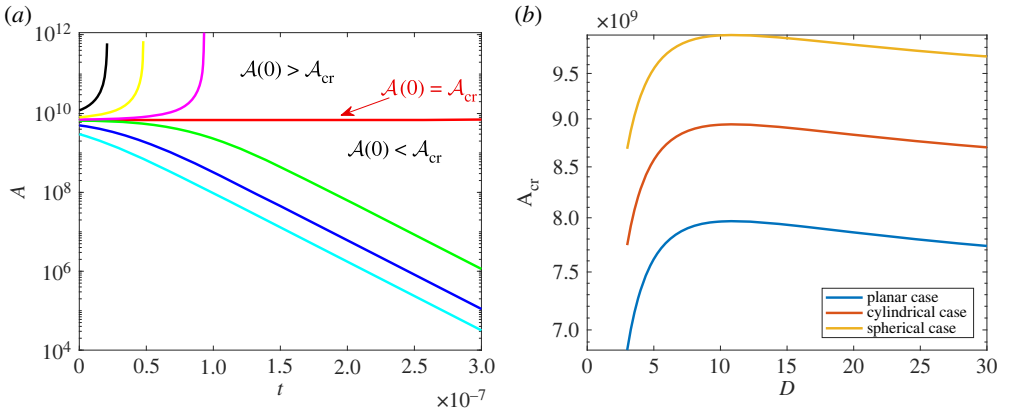

Figure 1. (*a*) Qualitative behaviour of the AW scalar amplitude as $\mathcal{A}(0)$ changes. (*b*) Critical amplitude in planar, cylindrical and spherical geometry of the outgoing fastest AW as a function of the molecular degrees of freedom. (Online version in colour.)

spherical form during its oscillation and its variable radius $R = R(t)$ is described by a nonlinear ordinary differential equation, the best-known is the Rayleigh–Plesset equation[3] [21,22]:

$$R\ddot{R} + \frac{3}{2}\dot{R}^2 = \frac{1}{\rho_f}\Big(P_g(R) - P_E + P_a(t)\Big) - \frac{4\eta\dot{R}}{\rho_f R} - \frac{2\varsigma}{\rho_f R} + \frac{R}{\rho_f c_f}\frac{\mathrm{d}}{\mathrm{d}t}(P_g(R) + P_a(t)), \tag{5.1}$$

where P_g denotes the pressure of the gas inside the bubble, P_a is the imposed sound field, c_f is the speed of sound in the fluid around the bubble, ρ_f indicates the mass density of such a fluid, η and ς are, respectively, the shear viscosity coefficient of the fluid and the surface tension, P_E is the ambient atmospheric pressure, which coincides with the equilibrium pressure of the gas if ς is neglected. The equation is derived through several simplifications: in particular, it is assumed that the bubble wall moves slower than both liquid and gas sound speeds. However, in many cases its validity is extended also to supersonic regimes when the velocity of the bubble wall exceeds the sound velocity [20–23]. We recall that (5.1) usually is associated with the homobaric hypothesis, i.e. assuming the gas pressure P_g inside the bubble to be spatially homogeneous. In this regard, some studies have shown that in reality the gas pressure inside the bubble, although not perfectly uniform (due to the acceleration of the bubble wall), can be considered as such, at least as a first approximation during expansion and early stages of the contraction of the bubble [36–38]. Moreover, concerning the final stages of a violent contraction of the bubble, the paper by Lin, Storey and Szeri shows how the inevitable non-uniformity of the gas pressure is compatible with the validity of the Rayleigh Plesset equation [24,39].

In the literature, the study about the bubble dynamics described by a Rayleigh–Plesset-type equation is carried out using two different approaches [24]. On the one hand, it is possible to express the gas pressure as a function of the radius of the bubble through some simplifying hypotheses (isothermal or adiabatic assumptions). In this way, the Rayleigh Plesset equation is closed and can be integrated as a stand-alone ODE in a very fast and simple way. An alternative technique for studying the bubble radius dynamics is that undertaken by Wu and Roberts [40,41], and then taken up by other authors, see for instance [36,37,42]: a Rayleigh Plesset-type equation is coupled with the differential equations describing the dynamics of the gas inside the bubble, and the resulting differential system is numerically integrated. This procedure could be much more onerous, especially if the integration is carried out for all the phases of the bubble dynamics, but it gives more accurate results. This second approach implies the problem of how to prescribe in (5.1) the value of P_g at the bubble interface. Among several proposals presented in the last

[3]The Rayleigh–Plesset equation was modified by many researchers, in order to take into account several physical effects. Here, we introduce one of its simplest forms, valid only when the system is far from van der Waals regime and the oscillations are not too strong.

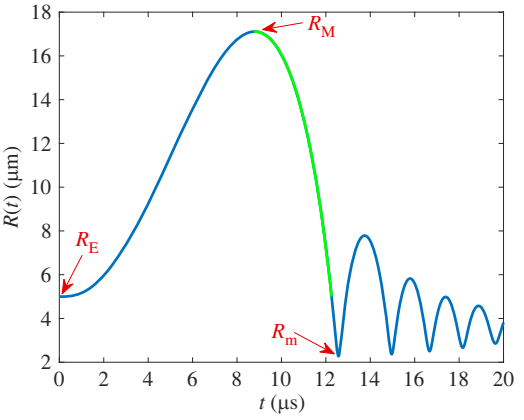

Figure 2. The qualitative behaviour of the radius of an oscillating gas bubble, described by Rayleigh–Plesset equation in the case of a monatomic gas. The green part of the plot represents the region taken into account in the present work. (Online version in colour.)

decades, we mention, among the others, the idea followed by Wu and Roberts [40,41] who place in the Rayleigh Lamb equation the value of the gas pressure at the bubble boundary $r = R$, the suggestions put forward by Prosperetti [36] and those recently presented by Man & Tuijillo in [38]. In this work, we refer to the first approach, postponing the second technique to a paper in preparation.

The qualitative behaviour of the bubble radius is shown in figure 2, starting from the value R_E that corresponds to the radius of the bubble in equilibrium with the fluid, when no external sound field is imposed. The bubble dynamics passes through different regimes in the presence of a periodic sound field, like $P_a = P'_a \cos(\omega_a t + \phi)$: an expansion up to the maximum radius R_M is followed by a contraction of the bubble sphere that reaches the equilibrium radius and further collapses to a minimum radius $R_m < R_E$ (in some cases, it could be of the magnitude order of the van der Waals hard core radius). A bouncing behaviour comes next, after the collapse. During the first phase of the contraction, when $R_M > R > R_E$, (5.1) is usually simplified, neglecting the gas pressure P_g, the acoustic pressure P_a and their variations, the viscous term and the surface tension, so that it is assumed [20–23]

$$\frac{1}{2}R^3\dot{R}^2 = \frac{P_E(R_M^3 - R^3)}{3\rho_f}. \tag{5.2}$$

In the present work, the analysis is restricted to this regime (where the gas can be modelled as a perfect gas).

The radius of the bubble varies in time ($R = R(t)$) and so does the domain in which the AWs propagate, i.e. the bubble sphere. To simplify the calculations, we consider the PDE model in spherical coordinates (2.6) and introduce a transformation from the usual time-space variables $\{t, r\}$ (with r radial coordinate inside the bubble $r \in [0, R(t)]$), to the more comfortable $\{t', x\}$ if $t' = t$ and $x = r/R(t)$ with $x \in [0, 1]$. So that, if $z = r$ denotes the radial variable, the PDE system (3.3) is transformed as follows:

$$\partial_t \mathbf{u} + \mathbf{A}\partial_z \mathbf{u} = \mathbf{T} \Rightarrow \partial_t \mathbf{u} + \frac{1}{R(t)}[\mathbf{A} - x\dot{R}\,\mathbf{I}]\partial_x \mathbf{u} = \mathbf{T}, \tag{5.3}$$

with $\dot{R} = \mathrm{d}R/\mathrm{d}t$. It is easily proved that the characteristic velocities (λ') of the transformed system $(5.3)_2$ are related to those (λ) of the initial system $(5.3)_1$ by $\lambda' = (\lambda - x\dot{R})/R(t)$. In addition to the monatomic ET^1_{13} and polyatomic $\mathrm{ET}^1_{14,P}$ equations, we introduce and analyse Euler's model (already employed within the bubble theory by several authors, see for example [17,40,41]).

(a) The rational extended thermodynamics model with 14 moments

Referring to the PDE system (2.6), assuming the space homogeneity so that $\sigma^{\langle 22\rangle} = -\sigma^{\langle 11\rangle}/2$ and taking into account that we are dealing with a spherical geometry $g = 2$, the number of equations reduces to six and the independent field variable vector becomes $\mathbf{u} = (\rho,\ v,\ \sigma,\ \Pi, p,\ q)$ if from now on we denote $\sigma^{\langle 11\rangle}$ by σ. The transformation described in (5.3) is easily applied, obtaining the final form of the PDE system

$$
\begin{aligned}
&\partial_t\rho + \frac{v - x\dot{R}}{R}\partial_x\rho + \frac{\rho}{R}\partial_x v = -\frac{2\rho v}{Rx},\\
&\partial_t v + \frac{v - x\dot{R}}{R}\partial_x v - \frac{1}{\rho R}\partial_x\sigma + \frac{1}{\rho R}\partial_x\Pi + \frac{1}{\rho R}\partial_x p = \frac{3\sigma}{\rho Rx},\\
&\partial_t\sigma + \frac{7\sigma - 4(p+\Pi)}{3R}\partial_x v + \frac{v - x\dot{R}}{R}\partial_x\sigma - \frac{8}{3(D+2)R}\partial_x q\\
&\quad = -\frac{8q}{3(D+2)Rx} - \frac{4(p+\Pi+2\sigma)v}{3Rx} - \frac{\sigma}{\tau_\sigma},\\
&\partial_t\Pi + \frac{2(D-3)(p-\sigma) + (5D-6)\Pi}{3DR}\partial_x v + \frac{v - x\dot{R}}{R}\partial_x\Pi + \frac{4(D-3)}{3D(D+2)R}\partial_x q\\
&\quad = -\frac{8(D-3)q}{3D(D+2)Rx} - \frac{2[(D-3)(2p+\sigma) + (5D-6)\Pi]v}{3DRx} - \frac{\Pi}{\tau_\Pi},\\
&\partial_t p + \frac{(D+2)p + 2\Pi - 2\sigma}{DR}\partial_x v + \frac{v - x\dot{R}}{R}\partial_x p + \frac{2}{DR}\partial_x q\\
&\quad = -\frac{4q}{DRx} - \frac{2(D+2)pv}{DRx} - \frac{4\Pi v}{DRx} - \frac{2\sigma v}{DRx},\\
&\partial_t q + \frac{p[-(D+2)p + (D+4)(\sigma - \Pi)]}{2R\rho^2}\partial_x\rho + \frac{2(D+5)q}{(D+2)R}\partial_x v - \frac{2(p+\sigma-\Pi)}{2R\rho}\partial_x\sigma\\
&\quad + \frac{2(p+\sigma-\Pi)}{2R\rho}\partial_x\Pi + \frac{(D+2)(p+\Pi-\sigma)}{2\rho R}\partial_x p + \frac{v - x\dot{R}}{R}\partial_x q\\
&\quad = -\frac{2(D+4)qv}{(D+2)Rx} + \frac{3(p+\sigma-\Pi)\sigma}{\rho Rx} - \frac{q}{\tau_q}.
\end{aligned}
\tag{5.4}
$$

We remark once again that system (5.4) reduces to the model of ET^1_{13} theory for a monatomic gas if one imposes $D = 3$ and neglects equation $(5.4)_4$, assuming $\Pi = 0$.

(b) The Euler model

The simplest RET theory used in the present physical framework is $\mathrm{ET}_{5,P}$, universally known as the Euler system. It can be obtained from the 14-moment model neglecting all the non-equilibrium field variables (stress tensor, dynamic pressure and heat flux) and their corresponding field equations. Referring to (5.4), the equations for an Euler gas reduce to

$$
\begin{aligned}
&\partial_t\rho + \frac{v - x\dot{R}}{R}\partial_x\rho + \frac{\rho}{R}\partial_x v = -\frac{2\rho v}{Rx},\\
&\partial_t v + \frac{v - x\dot{R}}{R}\partial_x v + \frac{1}{\rho R}\partial_x p = 0,\\
&\partial_t p + \frac{(D+2)p}{DR}\partial_x v + \frac{v - x\dot{R}}{R}\partial_x p = -\frac{2(D+2)pv}{DRx}.
\end{aligned}
\tag{5.5}
$$

The model is valid both for monatomic ($D = 3$) and for polyatomic gases $D > 3$.

(c) Preliminary assumptions

In what follows, we consider an AW generated by the bubble wall oscillation, acting as a piston on the gas. To deal with analytical or semi-analytical expression of Bernoulli's coefficients and AW amplitude equation, we introduce some further simplifications. First of all, we restrict the analysis to a linear time-dependence of the bubble radius

$$R(t) = R_0(1 + \mu t), \tag{5.6}$$

where R_0 is the initial bubble radius, while $\mu > 0$ represents the case of bubble expansion and $\mu < 0$ the linear contraction of the bubble. Due to this assumption, the analysis will be valid only for small time intervals. We postpone to the next paper the more realistic, but also more complex, nonlinear case.

In addition, we restrict our attention to unperturbed adiabatic solutions (i.e. $q = 0$) and impose that the unperturbed gas velocity presents a linear behaviour, that is $v = x\dot{R}$ (in some sense, the velocity of the gas is seen as a 'dragging' velocity caused by the bubble wall motion). Finally, the unperturbed stress tensor is supposed to be zero, in accordance with the unperturbed solution of the Euler system and also with the Navier–Stokes (NS) Fourier approximations, already employed by several authors (see for example [17,40–42]) for a gas confined in an oscillating bubble. To sum up, we consider an unperturbed solution ($\mathbf{u}_u$) that satisfies the conditions

$$v_u = x\dot{R}, \quad q_u = 0, \quad \sigma_u = 0. \tag{5.7}$$

The simplifying assumptions (5.6) and (5.7) imply the space uniformity of mass density, temperature, equilibrium and dynamic pressure, and allow an analytical description of the AW.

The unperturbed solution depends on some suitable integration constants: we have chosen to prescribe the initial values of equilibrium pressure p_0 and of mass density ρ_0 for both monatomic and polyatomic gases. We remark that $\mathrm{ET}^1_{14,P}$ theory requires the assignment of an additional quantity, such as Π_0 (initial dynamic pressure). Hereafter, the initial temperature T_0 is determined thanks to the ideal gas condition: $T_0 = p_0 m/(k_B \rho_0)$. Finally, we introduce a further simplifying hypothesis: the relaxation times τ_σ, τ_q and τ_Π are constant quantities, determined from (2.8) at established values of temperature and pressure.

(d) Notation

In what follows, we study first the AWs propagating in a bubble filled with a monatomic gas described by ET^1_{13} or Euler PDEs system. Then, we focus on the case of a polyatomic gas modelled by $\mathrm{ET}^1_{14,P}$ and Euler equations. To distinguish the quantities that refer to these theories, we introduce the following notation. A generic quantity w is written as: $\tilde{w}$ if it refers to the Euler model ET_5 with $D = 3$; $\tilde{\tilde{w}}$ if it corresponds to the Euler model $\mathrm{ET}_{5,P}$ when $D > 3$; $\hat{w}$ if it is described by ET^1_{13}; $\check{w}$ if it is associated with $\mathrm{ET}^1_{14,P}$ model.

6. Acceleration waves propagating in an oscillating bubble filled with a monatomic rarefied gas

The behaviour of the monatomic gas within the bubble is firstly described by the popular Grad's theory. Imposing conditions (5.7), system (5.4) reduces to the following set of PDEs and the

unperturbed fields are easily determined

$$\begin{aligned}&\partial_t\rho=-\frac{3\rho\dot{R}}{R},\\&\partial_x p=0,\\&\partial_t p=-\frac{5p\dot{R}}{R},\\&\frac{p}{\rho}\partial_x\rho-\partial_x p=0.\end{aligned}\qquad\Longrightarrow\qquad\begin{aligned}\hat{\rho}_u&=\frac{\rho_0}{(1+\mu t)^3}\\\hat{p}_u&=\frac{p_0}{(1+\mu t)^5}\end{aligned}\tag{6.1}$$

The dependence of the temperature field on the bubble radius turns out to be

$$\hat{T}_u=\frac{m\hat{p}_u}{k_B\hat{\rho}_u}=\frac{T_0R_0^2}{R^2(t)}.$$

The characteristic velocities $\hat{\lambda}'=\hat{\Lambda}+(v-x\dot{R})/R$ associated with ET^1_{13} can be determined from the knowledge of the roots $\hat{\Lambda}$ of the characteristic polynomial

$$\hat{P}(\hat{\Lambda})=0\Longleftrightarrow\hat{\Lambda}\Big(75\rho^2R^4\hat{\Lambda}^4+\hat{\Lambda}^2(310\sigma-390p)\rho R^2-288\hat{\Lambda}\rho Rq+(225p^2-450p\sigma+315\sigma^2)\Big)=0.$$

Thus, the characteristic speed of the fastest incoming wave propagating in the unperturbed solution is[4]

$$\hat{\lambda}_u=-\frac{1}{R}\sqrt{\left(\frac{13+\sqrt{94}}{5}\right)\frac{\hat{p}_u}{\hat{\rho}_u}}=\left(\frac{R_0}{R(t)}\right)^2\hat{\ell}_u,\quad\text{with }\hat{\ell}_u=-\sqrt{\left(\frac{13+\sqrt{94}}{5}\right)\frac{p_0}{\rho_0R_0^2}}.\tag{6.2}$$

and the corresponding right eigenvector associated with this system is given by $\hat{\mathbf{r}}_u=(\hat{r}_1,\hat{r}_2,\hat{r}_3,\hat{r}_4,\hat{r}_5)$ with $\hat{r}_2=-1/\hat{\lambda}_u$ (see §3) and

$$\hat{r}_1=\frac{\hat{r}_2\rho_u}{\hat{\lambda}_uR},\ \hat{r}_3=\frac{20\hat{r}_2(p_u^2-p_u\hat{\lambda}_u^2\rho_uR^2)}{\hat{\lambda}_uR(15\hat{\lambda}_u^2\rho_uR^2-33p_u)},\ \hat{r}_4=\frac{25\hat{r}_2(p_u\hat{\lambda}_u^2\rho_uR^2-p_u^2)}{\hat{\lambda}_uR(15\hat{\lambda}_u^2\rho_uR^2-33p_u)},\ \hat{r}_5=\frac{\hat{r}_245p_u^2}{15\hat{\lambda}_u^2\rho_uR^2-33p_u}.$$

The AW front is described, as usual, by the equation $\hat{\varphi}(x,t)=0$, which can be explicitly determined thanks to the linear time-dependence of the bubble radius (5.6). Recalling (6.2) and imposing that the wave front starts from the bubble wall at $x=1$, we have

$$\overset{\bullet}{\hat{\varphi}}=\partial_t\hat{\varphi}+\hat{\lambda}_u\partial_x\hat{\varphi}=0\Longrightarrow\hat{\varphi}(x,t)=x-1-\frac{\hat{\ell}_ut}{(1+\mu t)}.\tag{6.3}$$

Multiplying $\hat{\varphi}(x,t)$ by the expression of $R(t)$ in (5.6), we get $\hat{\Phi}=0$, i.e. the wave front equation in the original variables $\{t,r\}$:

$$\hat{\Phi}(t,r)=R(t)x-R(t)-R_0\hat{\ell}_ut=r-R_0-R_0(\mu+\hat{\ell}_u)t.$$

Hence, the AW propagates linearly inside the monatomic gas bubble with a speed that is equal to the sum of wall and characteristic velocities. This property holds for a monatomic Euler gas too. Bernoulli's coefficients are calculated from (3.4). Denoting by $\theta_0=k_BT_0/m$, they become

$$\hat{a}(t)=-\frac{5R\theta_0(-101\theta_0+235\hat{\ell}_u^2R_0^2)}{6R_0^4\hat{\ell}_u^3(34\theta_0+5\hat{\ell}_u^2R_0^2)}\simeq\frac{1.46776(1+\mu t)}{\sqrt{\theta_0}},$$

$$\hat{b}(t)=\frac{\nu_1\dot{R}}{R}+\frac{\nu_2}{\tau_\sigma}+\frac{\nu_3}{\tau_q}+\frac{\hat{\lambda}_u}{x}\simeq\frac{2\dot{R}}{R}+\frac{0.202793}{\tau_\sigma}+\frac{0.198429}{\tau_q}-\frac{2.13051R_0\sqrt{\theta_0}}{R(t)^2x}$$

with $$\nu_1=2,\ \nu_2=\frac{5(-\theta_0+\hat{\ell}_u^2R_0^2)^2}{\theta_0(-18\theta_0+72\hat{\ell}_u^2R_0^2)},\ \nu_3=\frac{3\hat{\ell}_uR_0^2}{-4\theta_0+16\hat{\ell}_u^2R_0^2}.$$

[4]Here, we focus on the AW with the fastest characteristic velocity, but the following results are valid in general for the waves propagating with non-zero characteristic velocities.

Recalling (3.2) and (6.3) and denoting by $c_1 = (\nu_2/\tau_\sigma) + (\nu_3/\tau_q)$, it is easily verified that

$$\hat{g}_1(t) = \frac{\exp(-c_1 t)}{(1+\mu t)(1+(\mu+\hat{\ell}_u)t)}$$

and

$$\hat{g}_2(t) = \frac{\hat{a}}{\mu+\hat{\ell}_u}\, \mathrm{e}^{c_1/(\mu+\ell_u)}\Delta\mathrm{Ei}(c_1, \hat{\ell}_u+\mu, t) \quad \text{with } \hat{a} = -\frac{5\theta_0(-101\theta_0 + 235\hat{\ell}_u^2 R_0^2)}{6\hat{\ell}_u^3 R_0^3(34\theta_0 + 5\hat{\ell}_u^2 R_0^2)}.$$

As mentioned before, the Euler system was already employed to describe the AW in an oscillating gas bubble. Here, we briefly summarize the main steps necessary to determine the AW amplitude described by ET_5, seen as a comparison term of the Grad's model. Concerning the unperturbed solution, under assumptions (5.7), the equations of the ET^1_{13} $(6.1)_{1,2,3}$ are valid also for an Euler gas. Since $(6.1)_4$ cannot be deduced from the ET_5 theory, the space dependence of ρ turns out to be arbitrary. However, the aim of this analysis is a comparison with the 13-moment system, so it is natural to impose $\tilde{\rho}_u = \hat{\rho}_u$, fulfilling a space uniformity requirement. In this way, one obtains identical unperturbed solutions of Euler's and Grad's models. In order to study the behaviour of the Euler AWs travelling inside the bubble, it is necessary to determine firstly the characteristic velocities $\tilde{\lambda}' = \tilde{\Lambda} + (v - x\dot{R})/R$ associated with this model. $\tilde{\Lambda}$ is a root of the characteristic polynomial $\tilde{\mathcal{P}}(\tilde{\Lambda}) = -\tilde{\Lambda}(-5p + 3\tilde{\Lambda}^2\rho R(t)^2)$, so that for ET_5 the characteristic speed of the fastest incoming AW and its value in the unperturbed solution are

$$\tilde{\lambda} = -\frac{1}{R}\sqrt{\frac{5}{3}\frac{p}{\rho}} + \frac{v - x\dot{R}}{R}, \quad \tilde{\lambda}_u = -\frac{1}{R(t)}\sqrt{\frac{5}{3}\frac{\tilde{p}_u}{\tilde{\rho}_u}} = \left(\frac{R_0}{R(t)}\right)^2 \tilde{\ell}_u \quad \text{with } \tilde{\ell}_u = -\sqrt{\frac{5p_0}{3\rho_0 R_0^2}}.$$

The unperturbed right eigenvector (denoted by $\tilde{\mathbf{r}}_u = (\tilde{r}_1, \tilde{r}_2, \tilde{r}_3)$) associated with the characteristic velocity of the incoming AW is defined as $\tilde{r}_1 = \tilde{r}_2\tilde{\rho}_u/(\tilde{\lambda}_u R(t))$, $\tilde{r}_3 = 5\tilde{r}_2\tilde{p}_u/(3\tilde{\lambda}_u R(t))$ where $\tilde{r}_2 = -1/\tilde{\lambda}_u$. The explicit expression of the AW front equation $\tilde{\varphi}(t,x) = 0$ presents the same form as the one of ET_{13} (6.3), with $\tilde{\ell}_u$ in place of $\hat{\ell}_u$. From (3.4), Bernoulli's coefficients can be easily deduced

$$\tilde{a}(t) = -\frac{4}{3\tilde{\lambda}_u R(t)} = -\frac{4(1+\mu t)}{3\tilde{\ell}_u R_0}, \quad \tilde{b}(t) = \frac{2\dot{R}}{R(t)} + \frac{\tilde{\lambda}_u}{x} = 2\frac{\mathrm{d}\ln(R(t))}{\mathrm{d}t} + \frac{\mathrm{d}\ln(x(t))}{\mathrm{d}t}.$$

and taking into account (3.2), we get

$$\tilde{g}_1(t) = \frac{1}{x(t)(1+\mu t)^2} \quad \text{and} \quad \tilde{g}_2(t) = -\frac{4(\ln(1+(\tilde{\ell}_u+\mu)t))}{3R_0\tilde{\ell}_u(\mu+\tilde{\ell}_u)}.$$

7. Acceleration waves propagating in an oscillating bubble filled with a polyatomic rarefied gas

In the case of an oscillating bubble filled with a polyatomic gas, described by the model in (5.4) and under conditions (5.7), the PDE system of the unperturbed fields becomes (we omit for

simplicity the identity relation corresponding to the equation $(5.4)_3$)

$$\begin{aligned}
&\partial_t\rho = -\frac{3\rho\dot{R}}{R},\\
&\frac{1}{\rho R}\partial_x(p+\Pi) = 0,\\
&\partial_t\Pi = -\frac{(2(D-3)p+(5D-6)\Pi)\dot{R}}{DR} - \frac{\Pi}{\tau_\Pi},\\
&\partial_t p = -\frac{3(D+2)}{DR}p\dot{R} - \frac{6\Pi\dot{R}}{DR},\\
&\frac{[(D+2)p+(D+4)\Pi]}{\rho}\partial_x\rho\\
&\quad - \frac{Dp+(D+4)\Pi}{p}\partial_x\Pi = 0,
\end{aligned}
\qquad\Longrightarrow\qquad
\begin{aligned}
&\check{\rho}_u = h(x)\left(\frac{R_0}{R(t)}\right)^3,\\
&\check{P}_u = \check{p}_u + \check{\Pi}_u = P_0H(t),\\
&\partial_t\check{\Pi}_u = -\frac{(2(D-3)\check{p}_u+(5D-6)\check{\Pi}_u)\dot{R}}{DR} - \frac{\check{\Pi}_u}{\tau_\Pi},\\
&\partial_t\check{p}_u = -\frac{3(D+2)}{DR}\check{p}_u\dot{R} - \frac{6\check{\Pi}_u\dot{R}}{DR},\\
&\partial_x\check{\rho}_u = \partial_x\check{p}_u = \partial_x\check{\Pi}_u = 0,
\end{aligned}
\tag{7.1}$$

where $h(x)$ and $H(t)$ are suitable functions of x and t, respectively. We stress that a zero dynamic pressure is incompatible with the previous equations, unless $\dot{R}=0$. This fact constitutes a relevant difference with respect to the monatomic case, but it is not very surprising. Even in the NS approximation the expected relation between Π and the gas velocity in spherical symmetry sounds [15]

$$\Pi_{NS} = -\nu\frac{\partial v^k}{\partial z^k} = -3\nu\frac{\dot{R}}{R}. \tag{7.2}$$

In one word, the oscillating bubble is a natural habitat for the dynamic pressure, even if we consider an oversimplified situation.

Through compatibility conditions ($\partial_{xt}\check{p}_u = -\partial_{xt}\check{\Pi}_u$, under the assumption of C^2 regularity of functions $\check{p}_u(x,t)$ and $\check{\Pi}_u(x,t)$) it is possible to prove from (7.1) that $\partial_x\Pi = \partial_x p = 0$ and consequently also $\partial_x\rho = 0$. Hence, conditions (5.6) and (5.7) imply space uniformity for $\mathrm{ET}^1_{14,P}$ unperturbed solution, in complete accordance with the results of ET^1_{13} for a monatomic gas. After some calculations, relations (7.1) can be rewritten as

$$\begin{aligned}
&\check{\rho}_u = \frac{\rho_0}{(1+\mu t)^3}, \quad \check{p}_u = p_0F(t),\ \check{\Pi}_u = \Pi_0G(t),\ \check{P}_u = \check{p}_u + \check{\Pi}_u,\\
&\Pi_0G(t) = -\frac{DRp_0}{6\dot{R}}\partial_tF(t) - \frac{(D+2)p_0}{2}F(t),\\
&\partial_t^2F(t) + \left[\frac{9\dot{R}}{R} + \frac{1}{\tau_\Pi}\right]\partial_tF(t) + \left[\frac{15\dot{R}^2}{R^2} + \frac{3(D+2)\dot{R}}{DR}\right]F(t) = 0.
\end{aligned}$$

To obtain an analytical solution, from now on we will focus on the case $D=6$, so that the unperturbed total pressure $\check{P}_u$ and the unperturbed dynamic pressure $\check{\Pi}_u$ turn out to be

$$\begin{aligned}
&\check{P}_u = \frac{\mathrm{e}^{-(t/\tau_\Pi)}(\check{c}_1 + \mu(t+2\tau_\Pi)\check{c}_1 - \mathrm{e}^{t/\tau_\Pi}\mu\tau_\Pi^2(-1-\mu t+2\mu\tau_\Pi)\check{c}_2)}{\mu(1+\mu t)^5\tau_\Pi}\\
&\text{and}\quad \check{\Pi}_u = \frac{\mathrm{e}^{-(t/\tau_\Pi)}(\check{c}_1 + \mu(t+\tau_\Pi)\check{c}_1 - \mathrm{e}^{t/\tau_\Pi}\mu^2\tau_\Pi^3\check{c}_2)}{\mu(1+\mu t)^5\tau_\Pi},
\end{aligned}
\tag{7.3}$$

where $\check{c}_1$ and $\check{c}_2$ are two suitable integration constants, which can be prescribed by the condition $P(t=0)=P_0$ and $\Pi(t=0)=\Pi_0$. The approximated relation (7.2) is employed to assign the uncontrollable value of the initial dynamic pressure as a function of the measurable total pressure ($\Pi_0 = -(\mu\tau_\Pi P_0)/(1-\mu\tau_\Pi)$ with $D=6$). So that it can be imposed

$$\check{c}_1 = \frac{P_0(\mu\tau_\Pi)^3}{1-\mu\tau_\Pi} \quad\text{and}\quad \check{c}_2 = \frac{P_0(1+\mu\tau_\Pi+\mu^2\tau_\Pi^2)}{\tau_\Pi(-1+\mu\tau_\Pi)}.$$

The expression of the unperturbed temperature field is deduced from (7.3), recalling that we deal with an ideal gas

$$\check{T}_u = T_0\left[\mathrm{e}^{-(t/\tau_\Pi)}\frac{\mu^3\tau_\Pi^3}{(1+\mu t)^2} + \frac{(1+\mu t-\mu\tau_\Pi)(1+\mu\tau_\Pi+\mu^2\tau_\Pi^2)}{(1+\mu t)^2}\right] \text{ with } T_0 = \frac{mP_0}{k_B\rho_0(1-\mu\tau_\Pi)}.$$

The characteristic velocities $\check{\lambda}' = \check{\Lambda} + (v - x\dot{R})/R$ of the $\mathrm{ET}^1_{14,P}$ are determined thanks to the characteristic polynomial equation

$$\check{\Lambda}^2[48\check{\Lambda}^4\rho^2R^4 - 4\check{\Lambda}^2\rho R^2(57p + 47(\Pi-\sigma)) - 99\check{\Lambda}q\rho R + 36(4p^2 + 8p(\Pi-\sigma) + 5(\Pi-\sigma)^2)] = 0.$$

Thus, the unperturbed speed of the fastest AW travelling towards the centre of the bubble described by $\mathrm{ET}^1_{14,P}$ turns out to be

$$\check{\lambda}_u = -\sqrt{\frac{57\check{p}_u + 47\check{\Pi}_u + \sqrt{1521\check{p}_u^2 + 1902\check{p}_u\check{\Pi}_u + 49\check{\Pi}_u^2}}{24\check{\rho}_uR^2}},$$

and the corresponding unperturbed right eigenvector is given by

$$\begin{aligned}
&\check{\mathbf{r}}_u = (\check{r}_1, \check{r}_2, \check{r}_3, \check{r}_4, \check{r}_5), \quad \check{r}_1 = \frac{\check{\rho}_u r_2}{R\check{\lambda}_u},\ \check{r}_2 = -\frac{1}{\check{\lambda}_u},\\
&\check{r}_3 = \check{r}_2\frac{4(4\check{P}_u^2 + \check{\Pi}_u^2 - 4\check{\lambda}_u^2\check{P}_u\check{\rho}_uR^2)}{\check{\lambda}_u^2R\delta_1},\\
&\check{r}_4 = -\check{r}_2\frac{4\check{P}_u^2 + \check{P}_u(21\check{\Pi} - 4\check{\lambda}_u^2\check{\rho}_uR^2) - 3\check{\Pi}_u(3\check{\Pi}_u + 4\check{\lambda}_u^2\check{\rho}_uR^2)}{\check{\lambda}_uR\delta_1},\\
&\check{r}_5 = -\check{r}_2\frac{16\check{P}_u^2 + 2\check{\Pi}_u(7\check{\Pi}_u + 6\check{\lambda}_u^2\check{\rho}_uR^2) - \check{P}_u(21\check{\Pi}_u + 16\check{\lambda}_u^2\check{\rho}_uR^2)}{\check{\lambda}_uR\delta_1},\\
&\check{r}_6 = \check{r}_2\frac{4(9\check{P}_u^2 - 10\check{P}_u\check{\Pi}_u - 3\check{\Pi}_u^2)}{\delta_1}, \quad \text{with} \quad \delta_1 = 12\check{\lambda}_u^2\check{\rho}_uR^2 - 21\check{P}_u + 10\check{\Pi}_u.
\end{aligned} \tag{7.4}$$

In this case, the equation of the AW front cannot be determined analytically

$$\dot{\check{\varphi}} = \partial_x\check{\varphi} + \check{\lambda}_u\partial_t\check{\varphi} = 0 \quad \text{so that } \partial_x\check{\varphi} = 1 \text{ and } x(t) = 1 + \int_0^t \check{\lambda}_u(s)\,\mathrm{d}s, \tag{7.5}$$

and one seeks help from a numerical procedure. After several calculations, Bernoulli's coefficients can be written as

$$\begin{aligned}
&\check{a} = -\frac{4\check{\lambda}_u^2\check{\rho}_uR^2(2412\check{P}_u^2 - 1355\check{P}_u\check{\Pi}_u - 447\check{\Pi}_u^2) - 9(584\check{P}_u^3 - 60\check{P}_u^2\check{\Pi}_u + 83\check{P}_u\check{\Pi}_u^2 + 15\check{\Pi}_u^3)}{3\check{\lambda}_u^3\check{\rho}_uR^3\delta_1\delta_2},\\
&\check{b} = \frac{\check{\nu}_1\dot{R}}{R} + \frac{\check{\nu}_2}{\tau_\sigma} + \frac{\check{\nu}_3}{\tau_q} + \frac{\check{\nu}_4}{\tau_\Pi} + \frac{\check{\lambda}_u}{x}, \qquad \text{with} \qquad \check{\nu}_1 = \frac{\check{\lambda}_u^2\delta_3 + \delta_4}{2\check{\lambda}_u^2\check{\rho}_uR^2\delta_1\delta_2\check{\Delta}^2},\\
&\check{\nu}_2 = \frac{8(3\check{P}_u + 2\check{\Pi}_u - 3\check{\lambda}_u^2\check{\rho}_uR^2)(4\check{P}_u^2 + \check{\Pi}_u^2 - 4\check{\lambda}_u^2\check{P}_u\check{\rho}_uR^2)}{9\check{\Delta}},\\
&\check{\nu}_3 = \frac{2\check{\lambda}_u^2(9\check{P}_u^2108\check{P}_u\check{\Pi}_u - 4\check{\Pi}_u^2)\check{\rho}_uR^2}{\check{\Delta}}, \quad \check{\nu}_4 = \frac{\check{\lambda}_u^2\delta_5 + \delta_6}{4\check{\lambda}_u^2\check{\rho}_uR^2\delta_1\delta_2\check{\Delta}},
\end{aligned}$$

where δ_1 is introduced in (7.4) and

$$\check{\Delta} = 4(33\check{P}_u^2 - 10\check{P}_u\check{\Pi}_u - 6\check{\Pi}_u^2)\check{\lambda}_u^2\check{\rho}_u R^2 - 5(3\check{P}_u + 2\check{\Pi}_u)(4\check{P}_u^2 + \check{\Pi}_u^2),\ \delta_2 = 24\check{\lambda}_u^2 R^2\check{\rho}_u - 57\check{P}_u + 10\check{\Pi}_u,$$

$$\begin{aligned}\delta_3 = {} & 1195807941\check{P}_u^8 - 2230441866\check{P}_u^7\check{\Pi}_u + 507998223\check{P}_u^6\check{\Pi}_u^2 + 762308496\check{P}_u^5\check{\Pi}_u^3 \\ & - 124802457\check{P}_u^4\check{\Pi}_u^4 - 113828422\check{P}_u^3\check{\Pi}_u^5 - 5412915\check{P}_u^2\check{\Pi}_u^6 + 3241188\check{P}_u\check{\Pi}_u^7 + 331668\check{\Pi}_u^8,\end{aligned}$$

$$\begin{aligned}\delta_4 = {} & -9(4\check{P}_u^2 + \check{\Pi}_u^2)(24867657\check{P}_u^7 - 39919740\check{P}_u^6\check{\Pi}_u + 1959970\check{P}_u^5\check{\Pi}_u^2 + 14213273\check{P}_u^4\check{\Pi}_u^3 \\ & + 506396\check{P}_u^3\check{\Pi}_u^4 - 1530052\check{P}_u^2\check{\Pi}_u^5 - 272928\check{P}_u\check{\Pi}_u^6 - 7968\check{\Pi}_u^7),\end{aligned}$$

$$\delta_5 = 12(10362\check{P}_u^5 - 25873\check{P}_u^4\check{\Pi}_u + 42328\check{P}_u^3\check{\Pi}_u^2 - 16424\check{P}_u^2\check{\Pi}_u^3 - 7524\check{P}_u\check{\Pi}_u^4 + 810\check{\Pi}_u^5)\check{\rho}_u R^2,$$

$$\delta_6 = -(4\check{P}_u^2 + \check{\Pi}_u^2)(23256\check{P}_u^4 - 48570\check{P}_u^3\check{\Pi}_u + 75826\check{P}_u^2\check{\Pi}_u^2 - 14145\check{P}_u\check{\Pi}_u^3 - 20286\check{\Pi}_u^4).$$

In the case of $\mathrm{ET}^1_{14,P}$ also the expressions of $\check{g}_1$ and $\check{g}_2$ cannot be determined analytically and are evaluated numerically.

The polyatomic gas could also be modelled by Euler conservation laws, neglecting *a priori* heat flux, stress tensor and dynamic pressure. The unperturbed field variables $\tilde{\tilde{\mathbf{u}}}_u = (\tilde{\tilde{\rho}}_u, x\dot{R}, \tilde{\tilde{p}}_u)$ must satisfy equations $(7.1)_{1,2,4}$ with null Π, and we impose space uniformity, as for Euler monatomic gases, so that, if $D = 6$

$$\tilde{\tilde{\rho}}_u = \frac{\rho_0}{(1+\mu t)^6},\quad \tilde{\tilde{p}}_u = \frac{p_0}{(1+\mu t)^4},\ \tilde{\tilde{T}}_u = \frac{m\tilde{\tilde{p}}_u}{k_B\tilde{\tilde{\rho}}_u} = \frac{T_0}{(1+\mu t)}.$$

When $D = 6$, the characteristic velocity of the incoming AW propagating in the unperturbed gas turns out to be $\tilde{\tilde{\lambda}}_u = 2\sqrt{\theta_0}/(\sqrt{3}R_0(1+\mu t)^{3/2}) = \tilde{\tilde{\ell}}_u/(1+\mu t)^{3/2}$ and the unperturbed right eigenvector $(\tilde{\tilde{\mathbf{r}}}_u = (-\tilde{\tilde{\rho}}_u/(\tilde{\tilde{\lambda}}_u^2 R(t)), -1/\tilde{\tilde{\lambda}}_u, -4\tilde{\tilde{p}}_u/(3\tilde{\tilde{\lambda}}_u^2 R(t)))$.

The equation of the wavefront becomes

$$x(t) - 1 - 2\frac{\tilde{\tilde{\ell}}_u}{\mu} + 2\frac{\tilde{\tilde{\ell}}_u}{\mu\sqrt{1+\mu t}} = 0.$$

The corresponding coefficients of Bernoulli's equation are

$$\tilde{\tilde{a}}_u = -\frac{7(1+\mu t)^{1/2}}{6R_0\tilde{\tilde{\ell}}_u}\quad \text{and}\quad \tilde{\tilde{b}}_u = \frac{7\dot{R}}{4R} + \frac{\tilde{\tilde{\lambda}}_u}{x(t)},$$

and they can be easily integrated in order to obtain an analytical expression of g_1 and g_2

$$\tilde{\tilde{g}}_1(t) = \frac{1}{(1+\mu t)^{7/4}x(t)},\quad \gamma_1 = 2\tilde{\tilde{\ell}}_u^2 + \tilde{\tilde{\ell}}_u\mu,\ \gamma_2 = 2\tilde{\tilde{\ell}}_u^2$$

and

$$\tilde{\tilde{g}}_2(t) = \frac{14}{3R_0\sqrt{\gamma_1\gamma_2}}\left[\ln\left(\frac{\sqrt{\gamma_1}(1+\mu t)^{1/4} + \sqrt{\gamma_2}}{\sqrt{\gamma_1}(1+\mu t)^{1/4} - \sqrt{\gamma_2}}\right) - \ln\left(\frac{\sqrt{\gamma_1} + \sqrt{\gamma_2}}{\sqrt{\gamma_1} - \sqrt{\gamma_2}}\right)\right].$$

The AW amplitude as a function of time is calculated in both models thanks to (3.2).

8. Analysis of the results and physical considerations

In §§6 and 7, we have already determined the equations of the AWs propagating in a contracting gas bubble modelled by RET theories. In what follows we will study some particular cases, comparing the predictions of different field equations, the results known in the literature and the effects due to different gas properties.

It was already stressed that the AW amplitude exhibits a peculiar mathematical singularity when $x(t) = 0$, which is to say when the wave front reaches the bubble centre. This fact would imply the shock formation of any AW with initial amplitude $\mathcal{A}(0) < 0$. However, a continuum theory is certainly not capable of predicting phenomena that take place at a spatial scale

comparable to a kinetic diameter $\mathfrak{d}$, or even less. In fact, from a physical standpoint the AW could bounce off and travel backwards before the radius of the wave front reaches $\mathfrak{d}$. To our knowledge, a theory capable of describing the AW behaviour in that framework is still lacking. In the following presentation, we will introduce the idea of a 'special' critical amplitude $\mathcal{A}^*_{\rm cr}$ that corresponds to the largest negative value of $\mathcal{A}(0)$ that gives rise to shock formation for $x(t) \geq \mathfrak{d}/R_0$, where R_0 is the initial radius of the spherical AW. Referring to (3.2), it is easily shown that

$$\exists t^* \in R^+ : \quad x(t^*) = \frac{\mathfrak{d}}{R_0} \quad \text{and} \quad \mathcal{A}^*_{\rm cr} = -\frac{1}{g_2(t^*)}.$$

Some of these critical values are presented in the next figures in order to investigate which are the physical conditions that support the appearance of a shock (we have chosen as sample value $\mathfrak{d} \simeq 2 \times 10^{-10}$ m, similar to the kinetic diameter of some common gas molecules).

The examples taken into account here are obtained imposing the following conditions.

AW propagation: the incoming AW starts from the bubble's wall when the radius of the bubble is R_0 ($R_M \geq R_0 \geq R_E$), and temperature and pressure of the gas inside the bubble are T_0 and P_0.

Bubble's parameters: the bubble is supposed to be initially in balance with the liquid with $R_E = 8.5 \times 10^{-6}$ m, $P_E = 10^5$ Pa, $T_E = 300$ K. Afterwards, a sound field activates the bubble's oscillation, giving rise to an expansion up to radius $R_M^{(1)} = 10R_E$ (*case 1*, compatible with SL) or $R_M^{(2)} = 3.5R_E$ (*case 2*, incompatible with SL). The present data are in agreement with those already known in the literature (e.g. [21,22]). The bubble velocity $\dot{R}$ and $\mu = \dot{R}/R_0$ in (5.6) are supposed to be constant during the AW propagation, and they are evaluated by (5.2) setting $R = R_0$.

Gas parameters: heat conductivity, shear viscosity and bulk viscosity are supposed to be linear functions of the temperature (interpolation functions of data deduced from [43–45]), but during the AW propagation toward the centre of the sphere these parameters are kept constant (at the initial temperature T_0), so that the relaxation times are constant too. The gas inside the bubble is a polyatomic one and the molecular degrees of freedom are prescribed to be $D = 3$ in the monatomic case and, for convenience, $D = 6$ in the polyatomic one. We remark that at room temperature D should be 5 for biatomic molecules and close to 7 for other polyatomic molecules.

Bubble's expansion and contraction: the preliminary bubble expansion (from R_E to R_M) is slow and commonly assumed to be isothermal [20–23]. Thus, when the bubble radius reaches R_M the gas temperature is $T_M = T_E$ and the gas pressure is given by $P_M = P_E(R_E/R_M)^3$ (in accordance with mass conservation). In case 1, if $R_0 \simeq R_M$, the corresponding pressure turns out to be very small $P_0 \simeq 100 \div 200$ Pa, i.e. we are dealing with a very highly rarefied gas or, it is the same, a very large Knudsen number. That case would be better described by kinetic theory or at least by an RET theory with many moments, rather than ET^1_{13}, ET^1_{14} or Euler systems. Concerning the subsequent contraction, it would be intermediate between an isothermal and an adiabatic transformation [21–23]. In the following analysis, we will suppose that the contraction is isothermal until the bubble radius reaches an assigned value R_a ($R_M \geq R_a \geq R_E$) with temperature $T_a = T_M = T_E$ and pressure $P_a = P_E(R_E/R_a)^3$; then we pass to an adiabatic regime (compatible with the calculations of the present work). In this regard, we have analysed two different scenarios. In *scenario A* $R_a \simeq R_M$: in this case, the isothermal condition is commonly prescribed, but the unperturbed solution shows small variation of the gas temperature and, so, adiabatic and isothermal behaviour are close to each other. On the contrary, *scenario B* focuses on the case in which R_a is close to R_E: the adiabatic hypothesis is physically more realistic under this condition [21–23], since the bubble wall moves faster.

With regard to the homobaric assumption described in §5, it is evident that the description of an AW travelling inside the bubble is incompatible with the hypothesis of a uniform gas pressure. However, from §3, it should be noted that the jump in the pressure derivative is $\mathcal{A}\hat{r}_4$ in the monatomic case (see §6) or $\mathcal{A}\check{r}_5$ (see §7) for a polyatomic gas. It is easily verified that these quantities remain small if the speed of the bubble wall is not too high. It has also been observed that during the bubble contraction the role of P_g in (5.1) can be neglected (see (5.2)) and we believe this is also the case for AW propagation. Moreover, we remark that the wave propagation time

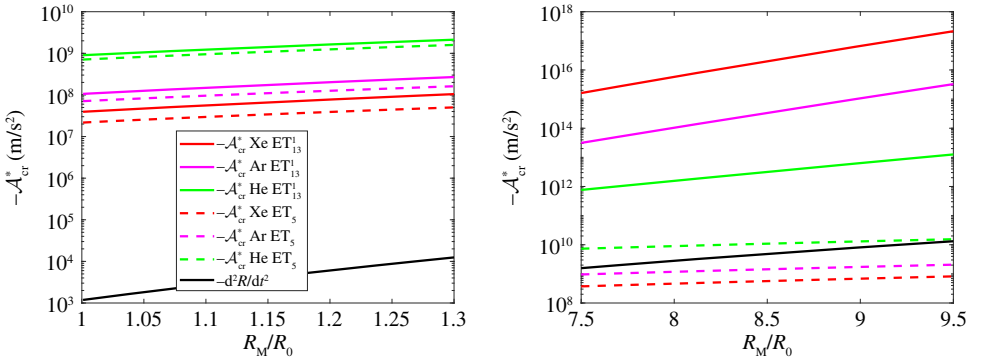

Figure 3. Case 1: $-\mathcal{A}^*_{cr}$ predicted by Euler's theory (dashed line) and by ET^1_{13} (continuous line) for different monatomic gases (He in green, Ar in magenta and Xe in red): on the left scenario A, on the right scenario B. The black line represents the opposite of the acceleration of the bubble wall estimated through (5.2). (Online version in colour.)

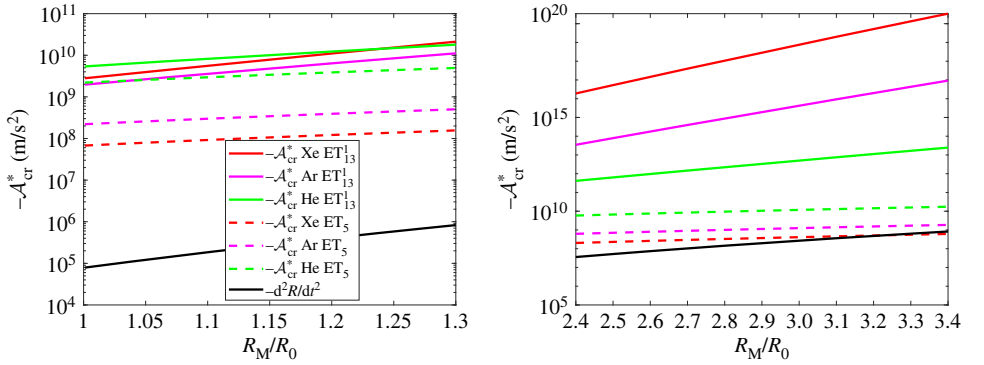

Figure 4. Case 2: $-\mathcal{A}^*_{cr}$ predicted by Euler's theory (dashed line) and by ET^1_{13} (continuous line) for different monatomic gases (He in green, Ar in magenta and Xe in red): on the left scenario A, on the right scenario B. The black line represents the opposite of the acceleration of the bubble wall estimated through (5.2). (Online version in colour.)

is very small by comparison with the oscillation time of the bubble, due to the high speed of the AW.

Figures 3 and 4 present the values of $|\mathcal{A}^*_{cr}|$ for an oscillating bubble containing a monatomic gas, described by ET_5 and ET^1_{13}, in case 1 and 2, respectively. The figures on the left are obtained in scenario A, while scenario B is taken into account in the figures on the right. Three different noble gases (helium, argon and xenon) are examined and compared. In all the figures, the absolute value of $\mathcal{A}^*_{cr}$ increases evidently passing from Euler's to Grad's predictions. Moreover, $\mathcal{A}^*_{cr}$ associated with ET^1_{13} differs by several orders of magnitude from the bubble wall acceleration, while in case 1 the Euler's special critical amplitude for Ar and Xe turns out to be substantially less than the estimated bubble wall acceleration (black line) when $R_0 \simeq R_E$. Thus, shock formation seems compatible with Euler's model, but not with ET^1_{13} theory. A final remark concerns the comparison of different gases: the smaller the atomic mass of the gas the higher the Aw velocity and consequently the values of $-\mathcal{A}^*_{cr}$ determined by Euler's system. This is not always the case with the Grad's prediction since a slower propagation could give enough time to the dissipation to act, at least when the gas is not too much rarefied. To this end, we recall that $m_{Xe} \simeq 33 m_{He}$ while $m_{Ar} \simeq 10 m_{He}$.

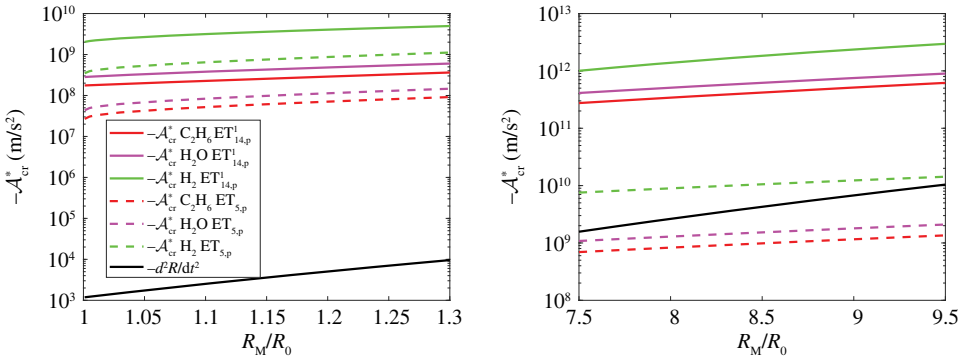

Figure 5. Case 1: $-\mathcal{A}^*_{cr}$ predicted by Euler's theory (dashed line) and by $ET^1_{14,P}$ (continuous line) for different polyatomic gases (H_2 in green, H_2O in magenta and C_2H_6 in red): on the left scenario A, on the right scenario B. The black line represents the opposite of the acceleration of the bubble wall estimated through (5.2). (Online version in colour.)

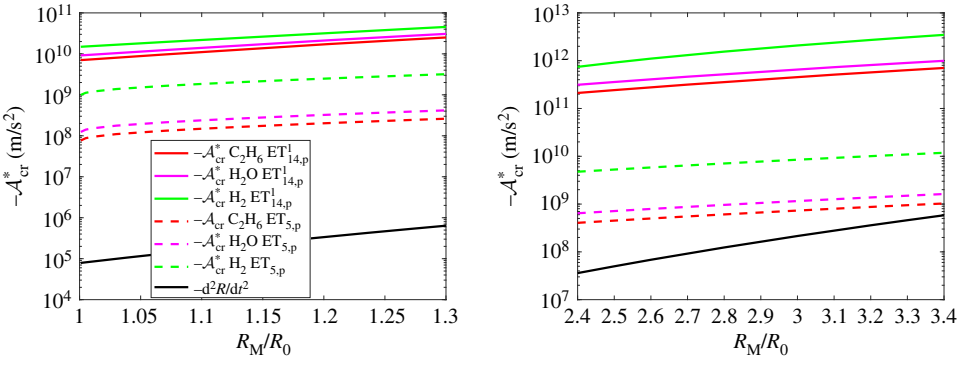

Figure 6. Case 2: $-\mathcal{A}^*_{cr}$ predicted by Euler's theory (dashed line) and by $ET^1_{14,P}$ (continuous line) for different polyatomic gases (H_2 in green, H_2O in magenta and C_2H_6 in red): scenario A on the left, scenario B on the right. The black line represents the opposite of the acceleration of the bubble wall estimated through (5.2). (Online version in colour.)

The examples of a bubble filled with a polyatomic gas are analysed in figures 5 and 6, where the results by $ET_{5,P}$ and $ET^1_{14,P}$ are compared for different gases (hydrogen, water vapour and ethane).[5] The plots suggest similar considerations as in the presence of a monatomic gas, although the relaxation times turn out to be shorter with respect to those of the monatomic gases, yielding sometimes slightly different effects. In general, if the dissipation is taken into account, the critical amplitude differs by some or even several orders of magnitude from the values determined by $ET_{5,P}$ and from the typical accelerations of the bubble wall.

Hence, we conclude that in both monatomic and polyatomic cases, shock formation becomes very unlikely and, accordingly, the unperturbed solutions tends to be stable, if one refers to RET models with dissipation.

The case of a bubble containing CO_2 gas has to be treated separately, due to the peculiarities of such a material. In the literature, the bulk viscosity ν of the carbon dioxide gas at room temperature is still a topic of debate. The values reported in [15,44,45,47–50] belong to a range of about $[0.5\mu_\upsilon, 5000\mu_\upsilon]$. The present physical framework is particularly sensitive to ν because of two different reasons connected with relaxation time and dynamic pressure. Firstly, different values of relaxation times correspond to different values of $\mathcal{A}^*_{cr}$, due to the combination of hyperbolicity

[5]The unperturbed solutions turn out to be always compatible with the hyperbolicity region of $ET^1_{14,P}$ [46].

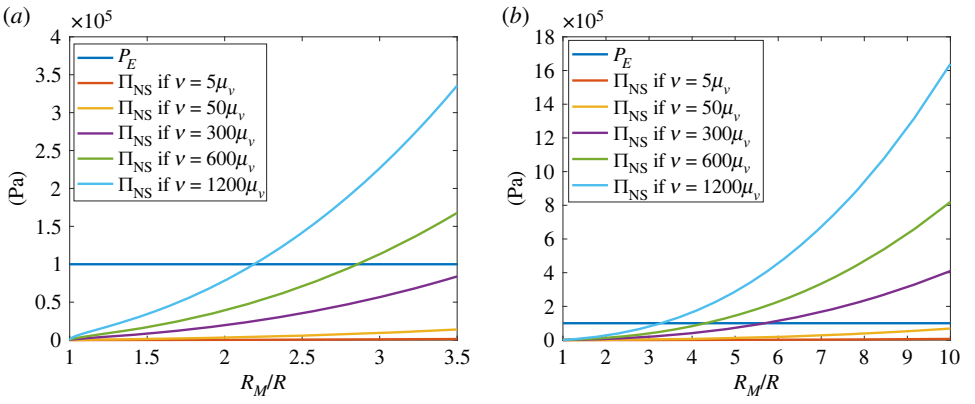

Figure 7. Comparison between the equilibrium pressure P_E and the dynamic pressure inside a CO_2 gas bubble in case 2 (on *a*) and in case 1 (on *b*) as a function of the ratio R_M/R, when different values of the ratio ν/μ_v are prescribed. The values of Π are obtained under isothermal assumptions and through Navier–Stokes approximation (7.2). (Online version in colour.)

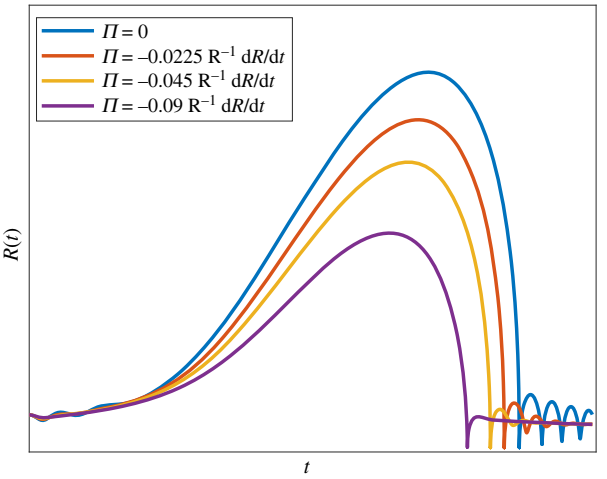

Figure 8. A rough sketch of a possible effect of dynamic pressure on the bubble radius dynamics $R(t)$ for a polyatomic gas with very high bulk viscosity. (Online version in colour.)

and dissipation. We do not present here the $\mathcal{A}^*_{cr}$ values, since they could be inconsistent with the approximations used in the present work. As a matter of fact, even if we prescribe isothermal conditions and NS approximation (7.2), as in figure 7, high values of the bulk viscosity give rise to uncontrollable very high values of the dynamic pressure in both case 1 and 2. Thus, Π is no more negligible with respect to P_E in (5.2) approximation, and one should take account of this quantity in Rayleigh–Plesset equation (5.1), as well. Physically, the possible high values of Π should oppose the bubble contraction and this effect could be observed in an experiment, giving an indirect measure of the bulk viscosity. A first oversimplified attempt to take into account the effect due to dynamic pressure in the Rayleigh–Plesset equation is presented in figure 8, where we have considered Π described by the NS approximation (7.2), for constant values of ν. The plot gives a rough qualitative idea of the phenomenon that could take place in a bubble entirely filled with a polyatomic gas that presents high bulk viscosity.

In addition, experimental data show that the presence of CO_2 gas inside the bubble inhibits the SL effect [51] and, in general, SL is less remarkable in bubbles containing polyatomic gases

[21,23]. Perhaps, besides other physical effects, there exists a correlation between SL and dynamic pressure.

Furthermore, it was already proved that dynamic pressure could give rise to observable effects in heat transfer [52] that takes place in spherical domains, and, therefore, it might not be neglected in bubble dynamics.

9. Conclusion and final remarks

In the present paper, we studied the behaviour of AWs propagating in a monatomic and a polyatomic gas, described by ET^1_{13} and $\mathrm{ET}^1_{14,P}$ theories. The role of wavefront geometry and the effect of the parameter D are presented here for the first time in the framework of RET. Section 4 can be seen as an extension of the results by Ruggeri & Seccia [8] in the case of a planar AW described by ET^1_{13} theory, and those by Lindsay & Straughan [5] obtained in several geometries with a rather different model. As a particular application of the AW theory, we focused on the case of a wave propagating inside an oscillating gas bubble within a liquid. In the last century, the phenomena occurring inside this type of bubbles have been extensively studied, both from theoretical and experimental standpoints. This peculiar physical framework presents extreme conditions, reached in very small space and time scales. Therefore, it constitutes a perfect test-bed for the AW studies and RET theory. In the past, several authors, starting from Greenspan and Nadim [17], have suggested that the AWs could play a special role in the SL formation. In this regard, we mention the work by Wu and Roberts [40,41] that represents a point of reference in the study of SL and was taken up by other authors. Other researchers, such as Vuong and Szeri, have subsequently questioned the shock formation and the possibility that SL is due to the conversion of an AW into a shock wave (e.g. [24,26,42,53,54]).

We believe that the results obtained through an RET model advance understanding of the processes occurring inside a gas bubble, even in SL conditions. In spite of the oversimplification of our first analysis, we have shown that hyperbolicity and dissipation make the conversion to shock wave much more difficult, also if the accelerations at stake are very high. In the scale range of validity of a continuum theory, we show that only a very large unrealistic initial amplitude of the AW can yield shock wave formation. Besides, this outcome was obtained under the adiabatic assumption, which is known to promote shock formation.

These analytical results highlight the fundamental role played by dissipation in the dynamics of the gas bubble. It is mathematically verifiable that thermal conductivity, shear and bulk viscosity prevent or slow down the transformation of the AWs into shock waves, so that one can speak of a stabilizing effect. More generally, the same phenomena could be observed in the eventual formation of shocks in the final stages of the gas bubble contraction. This question has already been dealt with by several authors, but without unanimity in the literature. Moreover, from the mathematical-physical standpoint, thanks to the hyperbolicity of RET equations, dissipation can take on a different role even than that predicted by the NS models. We are convinced that further comparisons should be carried on in the future.

The unperturbed solution presents unlike behaviours for monatomic and polyatomic gases, since $\Pi = 0$ is not compatible with this problem, also in the case of isothermal NS approximation. Under particular conditions of polyatomic gases with high bulk viscosity, the dynamic pressure could be an inhibiting factor of the bubble expansion during forced oscillation, interfering with SL as well. This could be the case of CO_2 gas. The effect has never been studied before, but it certainly deserves attention.

Regarding a possible comparison with experimental data, we start by saying that the available data refer to the analysis of the bubble radius during oscillations (see for instance [26]), and to measurements of the characteristics of the flash in the SL (e.g. [24]). Unfortunately, the experiments could lend themselves to different interpretations and a direct quantitative comparison turns out to be very difficult. However, it will be the subject of our planned research.

We stress that all the results were determined analytically or in a semi-analytical way and that graphics and numerical calculations were performed by MATLAB.

The possible extension of the present approach to more realistic and complex phenomena inside the oscillating gas bubbles will be the topic of our next paper, now in preparation.

Data accessibility. This article has no additional data.

Authors' contributions. F.B.: conceptualization, data curation, formal analysis, investigation, methodology, validation, visualization, writing—original draft, writing—review and editing; L.S.: conceptualization, data curation, investigation, methodology, validation, writing—original draft, writing—review and editing.

Both authors gave final approval for publication and agreed to be held accountable for the work performed therein.

Conflict of interest declaration. We declare we have no competing interests.

Funding. The paper was supported by Gruppo Nazionale di Fisica Matematica (GNFM) dell'INdAM and in part (F.B.) by the Italian research Project PRIN 2017 No. 2017YBKNCE 'Multiscale phenomena in Continuum Mechanics: singular limits, off-equilibrium and transitions.'

Acknowledgements. The authors would like to thank the anonymous reviewers for their helpful comments and suggestions.

Appendix A. Rational extended thermodynamics theory: truncation and closure of the equation system

As already mentioned in §2, the infinite hierarchies of balance laws obtained from the Boltzmann equation are commonly truncated at some truncation index (N for the F-series and M for the G-series) [15,55]. The truncation of the infinite sets of equations entails the question about how to express the last fluxes and the production terms as functions of the densities (seen as independent field variables): the so-called closure problem, whose solution comes from the MEP [15,56]. First of all through MEP, it is possible determine the equilibrium distribution function $f^{(E)}$ that maximizes the entropy

$$h = -k_B \int_{\mathbb{R}^3} \int_0^\infty f \ln f I^a dI d\mathbf{c}, \tag{A 1}$$

with the requirement that the hydrodynamic variables (mass density, momentum and energy: $\rho, \rho v_k, \rho v^2 + 2\rho\epsilon$) are expressed as moments of $f^{(E)}$. One refers to the Lagrange multipliers method and introduces the multipliers (u, u_k, u') (also called main field [14,15]) and the functional

$$\begin{aligned}\mathcal{L}_E = &-k_B \int_{\mathbb{R}^3} \int_0^\infty f \log f \, I^a \, dI d\mathbf{c} + u\left(\rho - \int_{\mathbb{R}^3} \int_0^\infty m f I^a dI d\mathbf{c}\right) \\ &+ u_k \left(\rho v_k - \int_{\mathbb{R}^3} \int_0^\infty m f c_k I^a dI d\mathbf{c}\right) + u'\left(\rho v^2 + 2\rho\epsilon - \int_{\mathbb{R}^3} \int_0^\infty m f \left(c^2 + 2\frac{I}{m}\right) I^a dI d\mathbf{c}\right).\end{aligned}$$

in the maximization of the functional with respect to f the same results are obtained referring to

$$\mathcal{L}'_E = \int_{\mathbb{R}^3} \int_0^\infty \left[-k_B \log f - m\left[u + u_k c_k + u'\left(c^2 + 2\frac{I}{m}\right)\right]\right] f I^a \, dI d\mathbf{c}.$$

Through the Euler–Lagrange equation $\delta\mathcal{L}'_E/\delta f = 0$, the equilibrium distribution function and the multipliers are easily determined

$$f^{(E)} = \frac{\rho}{mA(T)} \left(\frac{m}{2\pi k_B T}\right)^{3/2} \exp\left[-\frac{m}{k_B T}\left(\frac{C^2}{2} + \frac{I}{m}\right)\right] \quad \text{with } C_k = c_k - v_k,\ k = 1,2,3 \tag{A 2}$$

and

$$u^{(E)} = \frac{1}{T}\left(-g + \frac{v^2}{2}\right),\ u_k^{(E)} = -\frac{v_k}{T},\ u'^{,(E)} = \frac{1}{2T}, \quad A(T) = \int_0^\infty \exp\left(-\frac{I}{k_B T}\right) I^a dI, \tag{A 3}$$

where g denotes the chemical potential. In what follows, we will focus on the $\mathrm{ET}_{14,P}$ theory used in the present paper. Following the MEP procedure, it is possible to determine the correct

distribution function f corresponding to the 14-moment theory. Such a function maximizes the entropy (A 1) under the constraints that the moments F_A and $G_{llA'}$ are assigned as

$$F=\int_{\mathbb{R}^3}\int_0^\infty mfI^a\,dId\mathbf{c},\quad F_k=\int_{\mathbb{R}^3}\int_0^\infty mfc_kI^a\,dId\mathbf{c},\ F_{kj}=\int_{\mathbb{R}^3}\int_0^\infty mfc_kc_jI^a\,dId\mathbf{c}$$

and

$$G_{ss}=\int_{\mathbb{R}^3}\int_0^\infty mf\left(c^2+\frac{2I}{m}\right)I^a\,dId\mathbf{c},\quad G_{ssk}=\int_{\mathbb{R}^3}\int_0^\infty mf\left(c^2+\frac{2I}{m}\right)c_kI^a\,dId\mathbf{c}\ j,k=1,2,3.$$

Hence, the functional to be maximized can be written as

$$\mathcal{L}=\int_{\mathbb{R}^3}\int_0^\infty\left[-k_B\log f-m\left(u+u_kc_k+u_{kj}c_kc_j+(u'+u'_kc_k)(c^2+2\frac{2I}{m})\right)\right]fI^a dId\mathbf{c},$$

where u, u_k, u_{kj}, u', u'_k are the Lagrange multipliers associated with $F-$ and $G-$ moments.

Due the validity of the Galilean principle, one can refer equivalently to the following functional:

$$\mathcal{L}=\int_{\mathbb{R}^3}\int_0^\infty\left[-k_B\log f-m\left(\hat{u}+\hat{u}_kC_k+\hat{u}_{kj}C_kC_j+\left(\hat{u}'+\hat{u}'_kC_k\left(C^2+2\frac{2I}{m}\right)\right)\right)\right]fI^a dId\mathbf{C},$$

from now on the symbol $\hat{\cdot}$ denotes non-convective quantities (i.e. field variables evaluated when $\mathbf{v}=0$). After some calculations, the distribution function is given by

$$f=\exp(-1-\chi/k_B),\quad \text{with } \chi=\hat{u}+\hat{u}_kC_k+\hat{u}_{kj}C_kC_j+(\hat{u}'+\hat{u}'_kC_k)\left(C^2+2\frac{I}{m}\right). \tag{A 4}$$

The function f is usually approximated through the Taylor expansion of order $\alpha>0$ ($\alpha\in\mathbb{N}$) in the neighbourhood of a local equilibrium [15]

$$f^{(\alpha)}=f^{(E)}\left[1-\frac{m}{k_B}\bar{\bar{\chi}}+\frac{m^2}{2k_B^2}\bar{\bar{\chi}}^2+\cdots+(-1)^\alpha\frac{m^\alpha}{\alpha!k_B^\alpha}\bar{\bar{\chi}}^\alpha\right], \tag{A 5}$$

where

$$\bar{\bar{\chi}}=\chi-\chi^{(E)}=\bar{\bar{u}}+\bar{\bar{u}}_kC_k+\bar{\bar{u}}_{kj}C_kC_j+(\bar{\bar{u}}'+\bar{\bar{u}}'_kC_k)\left(C^2+2\frac{I}{m}\right)$$

$$\bar{u}=\hat{u}-\hat{u}^{(E)},\quad \bar{\bar{u}}'_k=\hat{u}'_k-\hat{u}'^{(E)}_k,\quad \bar{\bar{u}}'_{kj}=\hat{u}'_{kj}-\hat{u}'^{(E)}_{kj},\quad \bar{\bar{u}}'=\hat{u}'-\hat{u}'^{(E)},\quad \bar{\bar{u}}'_k=\hat{u}'-\hat{u}'^{(E)}_k,$$

and a quantity with apex $^{(E)}$ is evaluated at equilibrium. If we consider $\mathrm{ET}^1_{14,P}$ theory, prescribing $\alpha=1$, the non-convective multipliers turn out to be [15]

$$\hat{\hat{u}}=\frac{1}{T}(-g),\quad \hat{\hat{u}}_k=\frac{k_B\rho}{mp^2}q_k,\quad \hat{\hat{u}}_{kj}=-\frac{k_B\rho}{2mp^2}\left[-\sigma_{jk}+\frac{D}{D-3}\Pi\delta_{kj}\right]$$

and

$$\hat{\hat{u}}'=\frac{1}{2T}+\frac{3k_B\rho}{2(D-3)mp^2}\Pi,\quad \hat{\hat{u}}'_k=-\frac{k_B\rho^2}{(D+2)p^3}q_k,$$

and the last non-convective flux components (those not present in the list of the densities) are explicitly determined

$$\hat{\hat{F}}_{jkl}=\frac{D+2}{2}(q_j\delta_{kl}+q_k\delta_{jl}+q_l\delta_{jk}),\quad \hat{\hat{G}}_{ssjk}=\frac{D+2}{2}\frac{p^2}{\rho}\delta_{jk}-\frac{D+4}{2}\frac{p}{\rho}(\Pi\delta_{jk}-\sigma_{\langle jk\rangle}).$$

The convective components of the last fluxes are then determined through the Galilean invariance [57], obtaining (2.5).

References

1. Boillat G. 1965 *La propagation des ondes*. Paris: France Gauthier-Villars.

2. Boillat G, Ruggeri T. 1979 On the evolution of weak discontinuities for hyperbolic quasi-linear systems. *Wave Motion* **1**, 149–152. (doi:10.1016/0165-2125(79)90017-9)
3. Ruggeri T. 1989 Stability and discontinuity waves for symmetric hyperbolic systems. In *Nonlinear wave motion* (ed. A Jeffrey), pp.148–161. Harlow, UK: Longman Scientific and Technical.
4. Bowen RM, Doria ML. 1973 Effect of diffusion on the growth and decay of acceleration waves in gases. *J. Acoust. Soc. Am.* **53**, 75–82. (doi:10.1121/1.1913330)
5. Lindsay KA, Straughan B. 1978 Acceleration waves and second sound in a perfect fluid. *Arch. Ration. Mech. Anal.* **68**, 54–87. (doi:10.1007/BF00276179)
6. Jordan PM, Straughan B. 2006 Acoustic acceleration waves in homentropic Green and Naghdib gases. *Proc. R. Soc. A* **462**, 3601–3611. (doi:10.1098/rspa.2006.1739)
7. Muracchini A, Ruggeri T. 1989 Acceleration waves, shock formation and stability in a gravitating atmosphere. *Astrophys. Space Sci.* **153**, 127–142. (doi:10.1007/BF00643618)
8. Ruggeri T, Seccia L. 1989 Hyperbolicity and wave propagation in extended thermodynamics. *Meccanica* **24**, 127–138. (doi:10.1007/BF01559415)
9. Muracchini A, Seccia L. 1989 Thermo-acceleration waves and shock formation in extended thermodynamics of gravitational gases. *Contin. Mech. Thermodyn.* **1**, 227–237. (doi:10.1007/BF01171381)
10. Barbera E, Valenti G. 2006 Kawashima condition and acceleration waves for binary non reacting mixtures. *Acta Mech.* **187**, 203–217. (doi:10.1007/s00707-006-0379-7)
11. Brini F, Seccia L. 2020 Acceleration waves in rational extended thermodynamics of rarefied monatomic gases. *Fluids* **5**, 139. (doi:10.3390/fluids5030139)
12. Truesdell C, Noll W. 1965 *Handbuch der Physik*, III/3. Heidelberg: Springer.
13. Müller I. 2008 Extended Thermodynamics: a theory of symmetric hyperbolic field equations. *Entropy* **10**, 477–492. (doi:10.3390/e10040477)
14. Müller I, Ruggeri T. 1998 *Rational Extended Thermodynamics*. New York, NY: Springer.
15. Ruggeri T, Sugiyama M. 2021 *Classical and Relativistic Rational Extended Thermodynamics of gases*. New York, NY: Springer.
16. Arima T, Taniguchi S, Ruggeri T, Sugiyama M. 2012 Extended thermodynamics of dense gases. *Contin. Mech. Thermodyn.* **24**, 219–236. (doi:10.1007/s00161-011-0213-x)
17. Greenspan HP, Nadim A. 1993 On sonoluminescence of an oscillating gas bubble. *Phys Fluids A* **5**, 1065–167. (doi:10.1063/1.858619)
18. Lord Rayleigh OMFRS. 1917 On the pressure developed in a liquid during the collapse of a spherical cavity. *Phil. Mag. Ser.* **34**, 94–98. (doi:10.1080/14786440808635681)
19. Prosperetti A. 1982 Bubble dynamics: a review and some recent results. *Appl. Sci. Res.* **38**, 145–164. (doi:10.1007/BF00385945)
20. Prosperetti A, Hao Y. 1999 Modelling of spherical gas bubble oscillations and sonoluminescence. *Phil. Trans. R. Soc. A* **357**, 203–223. (doi:10.1098/rsta.1999.0324)
21. Löfstedt R, Barber BP, Putterman SJ. 1993 Toward a hydrodynamic theory of sonoluminescence. *Phys. Fluids A* **5**, 2911–2928. (doi:10.1063/1.858700)
22. Barber BP, Hiller RA, Löfstedt R, Putterman SJ, Weninger KR. 1997 Defining the unknowns of sonoluminescence. *Phys. Rep.* **281**, 65–143. (doi:10.1016/S0370-1573(96)00050-6)
23. Putterman SJ, Weninger KR. 2000 Sonoluminescence: how bubbles turns sound into light. *Annu. Rev. Fluid Mech.* **32**, 445–476. (doi:10.1146/annurev.fluid.32.1.445)
24. Brenner MP, Hilgenfeldt S, Lohse D. 2002 Single-bubble sonoluminescence. *Rev. Mod. Phys.* **74**, 425–484. (doi:10.1103/RevModPhys.74.425)
25. Suslick KS, Flannigan DJ. 2008 Inside a collapsing bubble: sonoluminescence and the conditions during cavitation. *Annu. Rev. Phys. Chem.* **59**, 659–683. (doi:10.1146/annurev.physchem.59.032607.093739)
26. Lauterborn W, Kurz T. 2010 Physics of bubble oscillations. *Rep. Prog. Phys.* **73**, 106501. (doi:10.1088/0034-4885/73/10/106501)
27. Borisenok VA. 2015 Sonoluminescence: experiments and models (Review). *Acoust. Phys.* **61**, 308–332. (doi:10.1134/S1063771015030057)
28. Crum LA. 2015 Resource paper: sonoluminescence. *J. Acoust. Soc. Am.* **138**, 2181–2205. (doi:10.1121/1.4929687)
29. Brennen CE. 2015 Cavitation in medicine. *Interface Focus* **5**, 20150022. (doi:10.1098/rsfs.2015.0022)
30. Borgnakke C, Larsen P. 1975 Statistical collision model for Monte Carlo simulation of polyatomic gas mixture. *J. Comput. Phys.* **18**, 405–420. (doi:10.1016/0021-9991(75)90094-7)

31. Bourgat JF, Desvillettes L, Tallec PL, Perthame B. 1994 Microreversible collisions for polyatomic gases. *Eur. J. Mech. B/Fluids* **13**, 237–254.
32. Boillat G. 1974 Sur l'existence et la recherche d'équations de conservation supplémentaires pour les systeèmes hyperboliques. *C. R. Acad. Sci. Paris* **278**, 909–912.
33. Ruggeri T, Strumia A. 1981 Main field and convex covariant density for quasi-linear hyperbolic systems. Relativistic fluid dynamics. *Ann. Inst. H. Poincaré Sect. A* **34**, 65–84.
34. Truesdell C. 1953 The physical components of vector and tensor. *ZAMM* **33**, 345–356. (doi:10.1002/zamm.19530331005)
35. Müller I. 1985 *Thermodynamics*. London, UK: New York Pitman.
36. Prosperetti A. 1991 The thermal behaviour of oscillating gas bubbles. *J. Fluid Mech.* **222**, 587–616. (doi:10.1017/S0022112091001234)
37. Zhou G, Prosperetti A. 2020 Modelling the thermal behaviour of gas bubbles. *J. Fluid Mech.* **901**, R3. (doi:10.1017/jfm.2020.645)
38. Man YAG, Trujillo FJ. 2016 A new pressure formulation for gas-compressibility dampening in bubble dynamics models. *Ultrasonics Sonochem.* **32**, 247–257. (doi:10.1016/j.ultsonch.2016.03.013)
39. Lin H, Storey BD, Szeri AJ. 2002 Inertially driven inhomogeneities in violently collapsing bubbles: the validity of the Rayleigh-Plesset equation. *J. Fluid Mech.* **452**, 145–162. (doi:10.1017/S0022112001006693)
40. Wu CC, Roberts PH. 1993 Shock-wave propagation in a sonoluminescencing gas bubble. *Phys. Rev. Lett.* **70**, 3424–3427. (doi:10.1103/PhysRevLett.70.3424)
41. Wu CC, Roberts PH. 1994 A model of sonoluminescence. *Proc. R. Soc. Lond. A* **445**, 323–349. (doi:10.1098/rspa.1994.0064)
42. Vuong VQ, Szeri AJ. 1996 Sonoluminescence and diffusive transport. *Phys. Fluids* **8**, 2354–2364. (doi:10.1063/1.869020)
43. Haynes WM. 2011 *CRC handbook of chemistry and physics*, 92nd edn. Boca Raton, FL: CRC Press.
44. Cramer MS. 2012 Numerical estimates for the bulk viscosity of ideal gases. *Phys. Fluids* **24**, 066102. (doi:10.1063/1.4729611)
45. Sharma B, Kumar R. 2019 Estimation of bulk viscosity of dilute gases using a nonequilibrium molecular dynamics approach. *Phys. Rev. E* **100**, 013309. (doi:10.1103/PhysRevE.100.013309)
46. Brini F, Ruggeri T. 2020 Hyperbolicity of first and second order extended thermodynamics theory of polyatomic rarefied gases. *Int. J. Non-linear Mech.* **124**, 103517. (doi:10.1016/j.ijnonlinmec.2020.103517)
47. Jaeger F, Matar OK, Müller EA. 2018 Bulk viscosity of molecular fluids. *J. Chem. Phys.* **148**, 174504. (doi:10.1063/1.5022752)
48. Kustova E, Mekhonoshina M, Kosareva A. 2019 Relaxation processes in carbon dioxide. *Phys. Fluids* **31**, 046104. (doi:10.1063/1.5093141)
49. Kosuge S, Aoki K. 2018 Shock-wave structure for a polyatomic gas with large bulk viscosity. *Phys. Rev. Fluids* **3**, 023401. (doi:10.1103/PhysRevFluids.3.023401)
50. Shang J, Wu T, Wang H, Xu W, Ye C, Hu R, Tao J, He X. 2020 Measurement of bulk viscosity of CO_2 based on spontaneous Rayleigh-Brillouin scattering. *IEEE Access* **8**, 40909–40917. (doi:10.1109/ACCESS.2020.2976883)
51. Kumari S, Keswani M, Singh S, Beck M, Liebscher E, Deymier P, Raghavan S. 2011 Control of sonoluminescence signal in deionized water using carbon dioxide. *Microelectron. Eng.* **88**, 3437–3441. (doi:10.1016/j.mee.2010.10.036)
52. Arima T, Barbera E, Brini F, Sugiyama M. 2014 The role of the dynamic pressure in stationary heat conduction of a rarefied polyatomic gas. *Phys. Lett. A* **378**, 2695–2700. (doi:10.1016/j.physleta.2014.07.031)
53. Vuong VQ, Szeri AJ, Young DA. 2001 Shock formation within sonoluminescence bubbles. *Phys. Fluids*, **11**, 10–17. (doi:10.1063/1.869920)
54. Lin H, Szeri AJ. 2001 Shock formation in the presence of entropy gradients. *J. Fluid Mech.* **431**, 161–188. (doi:10.1017/S0022112000003104)
55. Pavíc M, Ruggeri T, Simíc S. 2013 Maximum entropy principle for rarefied polyatomic gases. *Physica A* **392**, 1302–1317. (doi:10.1016/j.physa.2012.12.006)
56. Kogan M N. 1969 *Rarefied gas dynamics*. New York, NY: Plenum Press.
57. Ruggeri T. 1989 Galilean invariance and entropy principle for systems of balance laws: the structure of the extended thermodynamics. *Contin. Mech. Thermodyn.* **1**, 3–20. (doi:10.1007/BF01125883)